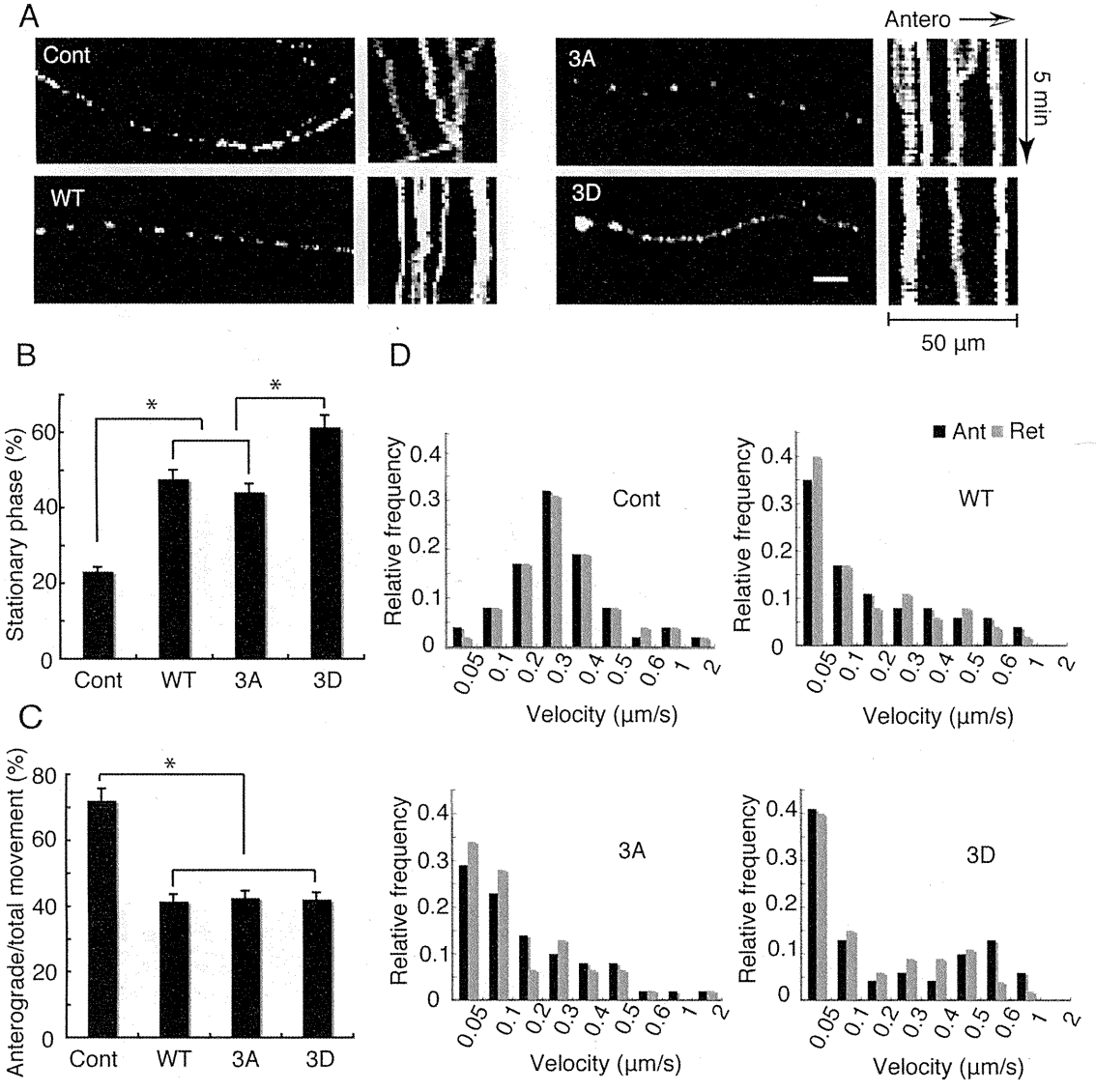

Figure 4. Effects of Tau WT, 3D, or 3A on mitochondrial movement in PC12 cells. ***A***, Mitochondrial distribution and movements in neurite process of PC12 cells. PC12 cells were transfected with a Mito-GFP vector alone as a control (Cont) or cotransfected with a Mito-GFP and Tau WT, 3A, or 3D vector. PC12 cells were treated with NGF for 72 h after transfection. Mitochondrial distribution is shown by fluorescence of Mito-GFP (left panels). Right panels are kymographs of mitochondria moving in a process of a PC12 cell. Antero, Anterograde. Bar, 20 μm. ***B***, The percentage ratio of pausing mitochondria in PC12 cell processes. Mitochondrial movement was recorded in the neurite-like processes at 5 s intervals over a 300 s period. Any mitochondrion that translocated at least 0.1 μm between two image frames was considered to be moving. The pausing time was expressed as the percentage of the total observation time ($n = 35$, $^*p < 0.01$, one-way ANOVA). ***C***, Effect of Tau WT, 3A, or 3D on anterograde or retrograde movement of mitochondria. The vertical axis indicates the ratio of anterogradely moving time to total moving duration. Statistical analysis was performed by ANCOVA as described in Materials and Methods. The ratio was significantly different between control and Tau-overexpressing PC12 cells ($^*p < 0.01$), but was not significant between three Tau constructs ($p = 0.75$). ***D***, Effect of Tau WT, 3D, or 3A on the velocity of mitochondria. Relative frequency of mitochondria moving at the indicated velocities in the anterograde (Ant, black) or retrograde (Ret, gray) direction for control, WT, 3A, or 3D. $n = 35$ mitochondria per sample.

The binding of kinesin to MTs is not affected by Tau in any phosphorylation state

Tau impairs mitochondrial movement by inhibiting the interaction of kinesin with MTs (Hagiwara et al., 1994). To delineate whether the reduced mitochondrial movement caused by Tau 3D expression was due to increased inhibition of the motor-MT interaction by Tau 3D, we examined the binding of the kinesin motor domain fragment RK430 to MTs in the presence of Tau WT, 3A, or 3D. We used the head domain of kinesin because the tail domain also has a MT-binding domain, which competes with Tau in *in vitro* MT-binding experiments (Seeger and Rice, 2010). Histidine-tagged kinesin (kinesin-His) that was bound or not bound to MTs was detected by Coomassie staining (Fig. 6*A*) and Western blotting (Fig. 6*B*) of the MT pellets and supernatants after centrifugation. Increasing the amount of Tau WT or Tau mutants did not alter the binding of RK430 kinesin-His to MTs even though excess Tau was added such that unbound Tau appeared in the supernatant. Thus, the reduced mitochondrial movement was not caused by inhibiting the interaction between the kinesin head domain and MTs.

The phosphorylation mimic Tau 3D increases MT spacing in processes of Sf9 cells

Tau is a space-making protein between MTs (Chen et al., 1992; Frappier et al., 1994; Marx et al., 2000). We examined the effect of phosphorylation at the AT8 sites on MT spacing *in vitro*. MTs were polymerized in the presence of Tau and pelleted by centrifugation. Thin-section electron micrographs of MTs cut perpendicularly to the MT axis are shown in Figure 7*A–C*. The inter-MT distances were

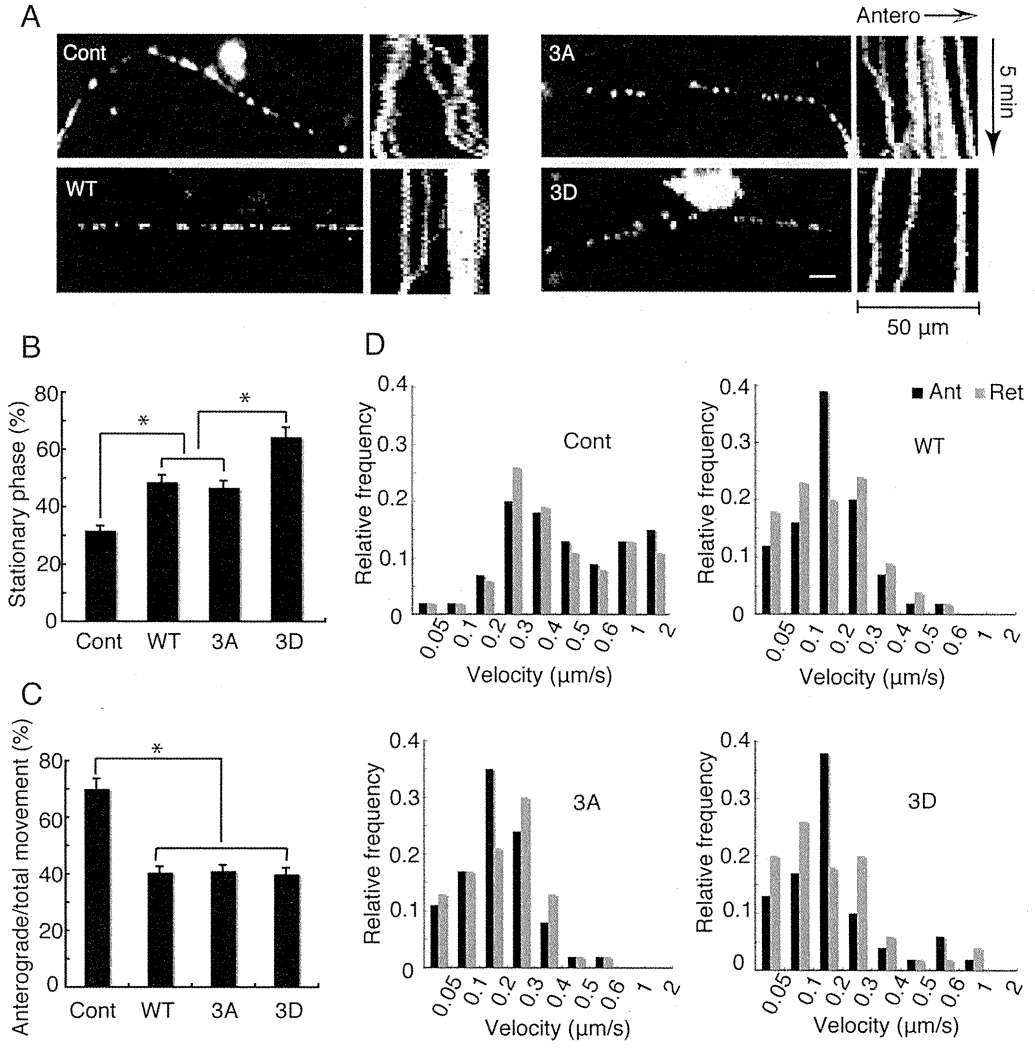

Figure 5. Reduced motile behavior of mitochondria in Tau-overexpressing neurons. ***A***, Mitochondrial distribution and movements in axons of neurons. Cultured neurons at DIV6 were transfected with Mito-GFP vector alone (Cont, Control) or cotransfected with Mito-GFP and Tau WT, Tau 3A, or Tau 3D vector. Mitochondrial distribution is shown by fluorescence of Mito-GFP (left panels). Bar, 20 μm. Right panels are kymographs of mitochondria moving in axon of neurons. Antero, Anterograde. ***B***, The percentage ratio of pausing mitochondria in axon of cultured neurons. The pausing duration was expressed as the percentage of total observation period ($n = 35$, $^*p < 0.01$, one-way ANOVA,). ***C***, The effect of Tau mutants on anterograde or retrograde movement of mitochondria. The vertical axis is the ratio of anterogradely moving duration to total moving period. The results were analyzed statistically by ANCOVA as described in Materials and Methods. The ratio was significantly different between control and Tau-overexpressing neurons ($p < 0.01$) but was not different between three Tau constructs ($p = 0.55$). ***D***, Effect of Tau mutants on the velocity of mitochondria. Relative frequencies of mitochondria moving at the indicated velocities are shown in control neurons or in neurons expressing Tau WT, Tau 3A, or Tau 3D. Black represents anterograde (Ant) movement, and gray represents retrograde (Ret) movement ($n = 35$ mitochondria per sample).

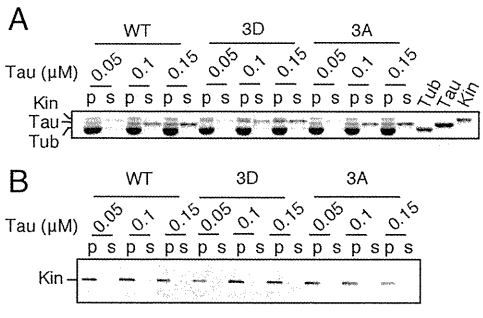

Figure 6. Tau does not inhibit the binding of kinesin to MTs. ***A***, Coomassie staining of an SDS-PAGE gel to show the binding of kinesin to MTs independent of Tau-binding. MTs polymerized in the presence of 0.05, 0.1, or 0.15 μM Tau WT, 3A, or 3D were incubated with 0.1 μM kinesin head domain-His and, after separation of MTs by centrifugation, the MT pellet (p) and supernatant (s) were subjected to SDS-PAGE. The right side three lanes are tubulin (Tub), Tau WT (Tau), and kinesin (Kin) head domain-His, respectively, for references. ***B***, An immunoblot confirming the binding of kinesin to MTs. MT pellet (p) and supernatant (s) shown in ***A*** are immunoblotted with anti-His antibody for detection of kinesin head domain-His.

measured from wall to wall of nearest-neighbor MTs. The distances were typically <10 nm in the MT pellets polymerized with Tau WT, 3A, and 3D (Fig. 7*D*), indicating that the phosphorylation-mimicking mutation at Ser199/Ser202/Thr205 did not affect the inter-MT spacing in pelleted MTs.

To determine whether this was the case in cells, we employed an Sf9 cell overexpression system that was used for Tau-induced MT bundle formation (Kanai et al., 1989; Frappier et al., 1994). We measured the distances between the nearest-neighbor MTs in the MT bundles formed in the process of Sf9 cells after infection of cells with baculovirus encoding Tau. Electron micrographs of processes in which most MTs were cut perpendicularly are shown in Figure 7, *E–G*, and the inter-MT distances are shown in Figure 7*H*. Of the 85 inter-MT distances measured, there was no significant difference between cells infected with the various Tau proteins (Fig. 7*H*). Because only a small number of processes were formed by Tau overexpression alone, however, the number of inter-MT distances we counted was not sufficient.

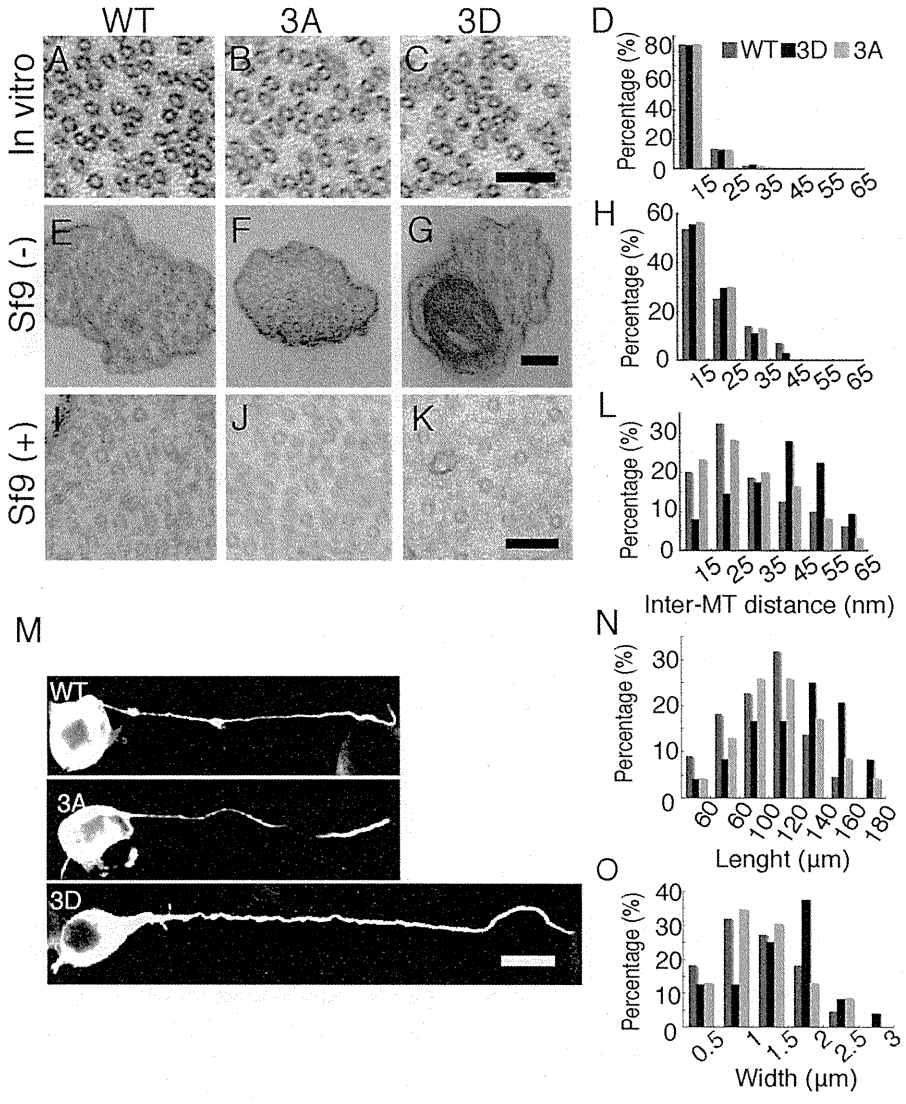

Figure 7. Inter-MT distance in MT bundles in the presence of Tau mutants. ***A–C***, Electron micrographs of cross-sections of MT pellets polymerized *in vitro* with Tau WT (***A***), 3A (***B***), or 3D (***C***). Scale bar, 100 nm. ***D***, The wall-to-wall distances between nearest-neighbor MTs were measured and expressed as the percentage of the total number of counted MTs. The mean distance was 11.7 ± 1.7 nm for Tau WT ($n = 48$), 11.8 ± 2.1 nm for Tau 3A ($n = 51$), and 11.9 ± 1.6 nm for Tau 3D ($n = 69$). ***E–G***, Electron micrographs of processes of Sf9 cells [untreated (−)] expressing Tau WT (***E***), 3A (***F***), or 3D (***G***). ***H***, Inter-MT distances were measured between nearest-neighbor MTs and expressed as the percentage of the total number of counts. The mean distance was 15.7 ± 2.2 nm for Tau WT ($n = 30$), 17.5 ± 2.7 nm for Tau 3A ($n = 27$), and 16.3 ± 2.2 nm for Tau 3D ($n = 28$). *I–K*, Electron micrographs of processes of latrunculin B-treated (+) Sf9 cells expressing Tau WT (***I***), 3A (***J***), or 3D (***K***). Sf9 cells were treated with 0.5 μg/ml latrunculin B for 72 h after infection with baculovirus expressing each Tau. ***L***, Inter-MT distances were measured and expressed as the relative ratio of the total number of counts. The mean distance was 26.8 ± 2.7 nm for Tau WT ($n = 60$), 27.2 ± 2.0 nm for Tau 3A ($n = 80$), and 37.1 ± 2.3 nm for Tau 3D ($n = 75$). ***M***, Immunostaining of Sf9 cells overexpressing Tau 3D (top), Tau 3A (middle), or WT (bottom) with anti-Tau. Scale bar, 20 μm. ***N, O***, Sf9 cells overexpressing Tau 3D formed longer and wider processes compared to those expressing Tau WT or 3A. ***N***, The length distribution of Sf9 cell processes overexpressing Tau constructs. The mean length was 106.5 ± 3.7 μm for Tau WT, 97.2 ± 5.3 μm for Tau 3A, and 119.1 ± 4.3 μm for Tau 3D ($n = 20$ for each Tau construct). ***O***, The width distribution of Sf9 cell processes overexpressing Tau constructs. The mean width was 1.09 ± 0.04 μm for Tau WT, 1.04 ± 0.09 μm for Tau 3A, and 1.39 ± 0.07 μm for Tau 3D ($n = 20$ for each Tau construct).

We therefore treated Tau-overexpressing Sf9 cells with latrunculin B, which disrupts actin filaments, to increase the number of processes (Knowles et al., 1994). When the processes were stained with anti-Tau antibody, we noticed that Sf9 cells expressing Tau 3D had larger and longer processes than cells expressing Tau WT or 3A (Fig. 7*M–O*). The mean length was 106.5 ± 3.7 μm for Tau WT, 97.2 ± 5.3 μm for Tau 3A, and 119.1 ± 4.3 μm for Tau 3D (Fig. 7*N*). The mean diameter was 1.09 ± 0.04 μm for Tau WT, 1.04 ± 0.09 μm for Tau 3A, and 1.39 ± 0.07 μm for Tau 3D (Fig. 7*O*). We then observed MTs in processes by electron microscopy (Fig. 7*I–K*). The inter-MT distances were greater in Tau 3D-overexpressing cells compared to those overexpressing WT or 3A (Fig. 7*L*). Although most distances fell in the range of 15–25 nm in Tau WT- and 3A-expressing cells (mean distance = 26.8 ± 2.7 and 27.2 ± 2.0 nm, respectively), almost same as the previous results (Frappier et al., 1994), that range was 35–45 nm in Tau 3D-expressing cells (mean distance = 37.1 ± 2.3 nm) (Fig. 7*L*). Because latrunculin B reduces membrane tension by depolymerizing submembranous actin filaments, these results suggested that, under reduced tension, phosphorylation of Tau at the AT8 sites increases the space between MTs.

Tau overexpression reduces the inter-MT distances in neurites of PC12 cells

We wanted to know how expression of Tau 3A or 3D affects the inter-MT distance in axons or neuritic processes. We performed

the experiments with PC12 cells in which mitochondrial movements were affected by Tau expression as was observed in neuronal axons. Typical electron micrographs are shown in Figure 8A. More MTs were found in neurites of PC12 cells overexpressing Tau. The inter-MT distances were reduced to ~35 nm in Tau-expressing processes from ~45 nm in the control untransfected processes (Fig. 8*B*). In contrast, there was no significant difference in the inter-MT distances among Tau WT, 3A, and 3D overexpression (Fig. 8*B*). The mean distance was 33.1 ± 2.4 nm for Tau WT, 34.1 ± 2.6 nm for Tau 3A, and 34.19 ± 2.8 for 3D.

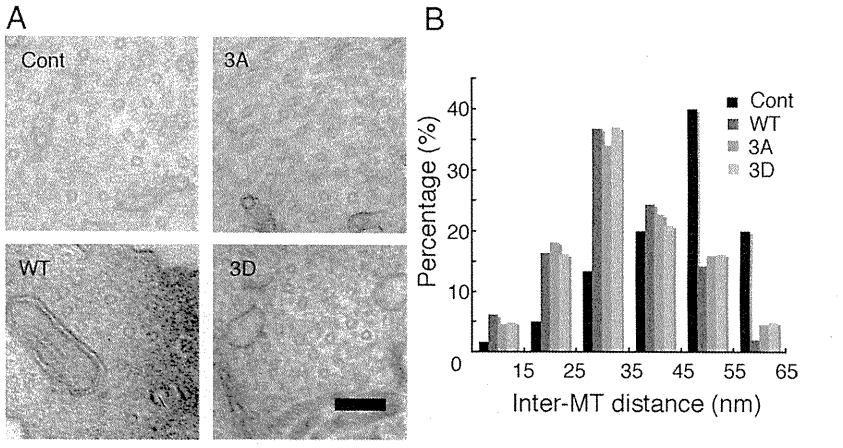

Figure 8. The distance between MTs in PC12 cell neurites overexpressing Tau constructs. ***A***, Cross-sectional electron micrographs of PC12 cell neurites, control (Cont) or overexpressing Tau WT, 3A, or 3D. Scale bar, 100 nm. ***B***, Inter-MT distances were measured between nearest-neighbor MTs and expressed as the percentage of the total number of counts. The mean distance was 45.1 ± 2.2 ($n = 54$) for control PC12 cells and 33.1 ± 2.4 nm ($n = 49$), 34.1 ± 2.6 nm ($n = 44$), and 34.19 ± 2.8 nm ($n = 62$) for PC12 cells overexpressing Tau WT, 3A, and 3D, respectively.

Discussion

Tau is a major MAP in axons and plays a role in regulating organelle transport and the dynamics of axonal MTs. Many reports have described the inhibition of mitochondrial transport by overexpressing Tau (Ebneth et al., 1998; Trinczek et al., 1999; Stamer et al., 2002; Dixit et al., 2008; Dubey et al., 2008; Stoothoff et al., 2009; Vossel et al., 2010). However, the molecular mechanism has not been determined. We studied the effect of AT8 Alzheimer phosphorylation (Ser199/Ser202/Thr205) of Tau on mitochondrial movement and found that the phosphorylation mimetic form, Tau 3D, inhibited mitochondrial transport to a greater degree than Tau WT and Tau 3A. Based on these findings together with the observation that the inter-MT distance was greater in MT bundles containing Tau 3D, we would like to propose that phosphorylation of Tau at the AT8 sites affects the transport of mitochondria along MTs by changing the inter-MT spaces.

Tau is a phosphoprotein with multiple phosphorylation sites; mass spectroscopic analysis indicates ten and five major sites in fetal and adult rat brains, respectively (Watanabe et al., 1993; Morishima-Kawashima et al., 1995; Planel et al., 2002). Major phosphorylation sites are in the Ser-Pro and Thr-Pro sequences, and most of them are in the region flanking the MT-binding domain. Phosphorylation at these sites reduces, but does not abolish, Tau binding to MTs, leading to more dynamic MTs (Wada et al., 1998; Liu et al., 2007). However, site-specific functions have not been completely investigated. Among the many Ser/Thr phosphorylation sites, Ser199, Ser202, and Thr205, which contain the recognition epitope for the AT8 monoclonal antibody, are particularly interesting. The AT8 sites are not only physiological phosphorylation sites (Kimura et al., 2007; Verwer et al., 2007) but also markers of hyperphosphorylation in Alzheimer's disease (Plattner et al., 2006). The Ser199/Ser202/Thr205 sites are present in the border between the N-terminal projection region and the MT-binding region. According to the paperclip structural model of Tau (Jeganathan et al., 2006), the site near Ser199/Ser202/Thr205 folds and the N-terminal region is situated close to the MT-binding repeats. When the Ser199/Ser202/Thr205 sites are phosphorylated the N-terminal domain swings away from the C-terminal domain, resulting in a conformation that extends from the MT wall (Jeganathan et al., 2008). The extended projection may increase the distance between MTs, although this idea has not been validated. By observing MT bundles in Sf9 cell processes treated with latrunculin B, we found that the inter-MT distance in MT bundles containing Tau 3D was longer than that in MT bundles containing Tau WT or Tau 3A.

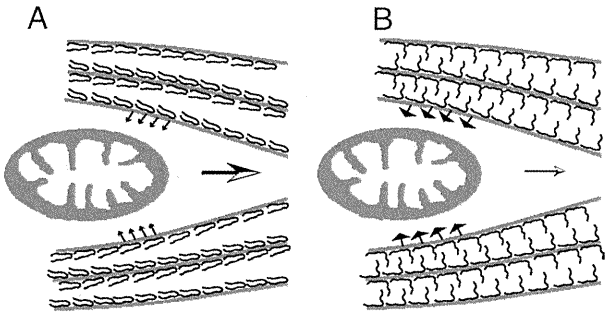

Figure 9. Schematic representation of the greater impact of Tau phosphorylation on mitochondrial transport compared to nonphosphorylated Tau. ***A***, Tau is a space-making protein attached to the MT surface. When Tau is not phosphorylated at Ser199/Ser202/Thr205, the N-terminal domain is folded. This conformation does not produce much resistance force against mitochondrial movement because MTs are in relatively close proximity. ***B***, Tau phosphorylation at Ser199/Ser202/Thr205 may extend the projection domain away from the MT surface, increasing the repulsive forces between MTs. In this conformation, mitochondria encounter greater MT resistance to the slowing or arresting of their movement.

Tau overexpression inhibits mitochondrial movement in various cell types (Ebneth et al., 1998; Trinczek et al., 1999; Stamer et al., 2002; Dixit et al., 2008; Stoothoff et al., 2009; Vossel et al., 2010). We also observed an inhibition of mitochondrial movement in PC12 cells and cortical neurons. Tau WT overexpression increased the pausing frequency from 31.6 to 48.5% in neurons, which is almost identical to previous results (Stamer et al., 2002). Overexpression of either Tau WT, 3A, or 3D reduced anterograde movement of mitochondria in PC12 cells and cortical neurons, as reported (Mandelkow et al., 2004; Hollenbeck and Saxton, 2005; Dixit et al., 2008). Furthermore, the velocity was reduced similarly in both directions by Tau overexpression regardless of its phosphorylation state, although the inhibition profile differed slightly among the three Tau constructs. Thus, Tau clearly inhibits mitochondrial transport independent of its phosphorylation state. Several models have been proposed for Tau-mediated inhibition of mitochondrial transport: overstabilization of MTs (Shemesh et al., 2008), competition between motor proteins for interaction with the MT surface (Hagiwara et al., 1994), and in-

hibition of motor protein access to MTs (Seeger and Rice, 2010). Another mechanism proposed recently involves the distance between MTs (Thies and Mandelkow, 2007). When Tau is overexpressed in cortical neurons, tubulin synthesis is upregulated and MTs become more numerous and densely packed, resulting in inhibition of mitochondrial movement. This observation was in dendrites, but similar Tau overexpression-induced increases in MTs were reported in axons (Sudo and Baas, 2010). We observed here that Tau overexpression increased the number of MTs and reduced the inter-MT spaces in neurites of PC12 cells. Our observation is consistent with the last model described above. Considering that mitochondria would be transported within MT bundles in cultured neurons (Yu and Baas, 1994; Rochlin et al., 1996), limited spacing between MTs may block mitochondrial movement in neuritic processes such as axon and dendrites.

We found that Tau 3D more potently inhibited mitochondrial transport than Tau WT or Tau 3A. Phosphorylation of Tau at the AT8 sites has an additional inhibitory action on mitochondrial movement over the Tau molecule itself. We hypothesize that the inhibition caused by Ser199/Ser202/Thr205 phosphorylation relates to the distance between MTs. The inter-MT distance was the same (15–25 nm) in MT bundles formed by Tau WT, 3A, and 3D in Sf9 cell processes, but it was expanded to 35–45 nm in processes expressing Tau 3D when actin filaments were disrupted by latrunculin B. Actin filaments are abundant in submembranous regions, providing tension to plasma membranes. As reported (Knowles et al., 1994), disassembly of actin filaments increases the number of processes induced by Tau overexpression. Phosphorylation-dependent expansion of the space between MTs was observed only with reduced membrane tension. The force produced by outward extension of the projection domain may not be strong enough to push surrounding MTs against the membrane, which may explain why phosphorylation-induced expansion of the inter-MT distance has not been reported.

Axons are long processes that extend ~1 m or more. To maintain axonal structures to over 80 years in humans, the axoplasm is filled with cytoskeletal components, and the outer surface is surrounded by thick myelin. These features may indicate that the axoplasmic MT milieu is under the strong tension (Yu and Baas, 1994; Rochlin et al., 1996). Phosphorylation of Tau at the AT8 sites tends to increase the inter-MT distance, but under strong tension the inter-MT distance cannot expand (Fig. 8), and instead the repulsive forces between MTs increase (Fig. 9). Increased repulsive forces between MTs would generate a stronger reactive resistance against mitochondria moving inside MT bundles. The AT8 sites are physiological sites for phosphorylation, but they are not always phosphorylated (Kimura et al., 2007; Verwer et al., 2007). The AT8 sites may be interconverted between phosphorylated and dephosphorylated states depending on the cell's need for mitochondrial movement. Dephosphorylation ahead of moving mitochondria would reduce the repulsive force between adjacent MTs for mitochondrial passage, and rephosphorylation of Tau behind mitochondria may facilitate the directional movement of mitochondria (Shahpasand et al., 2008). Of course, phosphorylation-dependent tunnel opening and closing for mitochondrial movement is expected to be coordinated with activities of motor proteins, protein kinases, and protein phosphatases. This is our working hypothesis, which we will explore further in the future.

We used PC12 cells and cultured cortical neurons in this study in which MTs are major cytoskeletal components. In matured or aged neurons, however, Tau may not be the only space-making protein that affects mitochondrial movement in a phosphorylation-dependent manner. The C-terminal tail domains of neurofilament M and H subunits extrude outward from core filaments, as does the projection domain of Tau, to make spaces between neurofilaments (NFs) (Hisanaga and Hirokawa, 1989). NFs are highly phosphorylated in aged axons and AD neurodegenerative disease (Uchida et al., 2004; Rudrabhatla et al., 2010). Hyperphosphorylation of the tail domains would increase the inter-NF distances to expand the NF domain in axons (Kumar et al., 2002; Kanungo et al., 2011), giving higher pressure to the MT domain. This would suppress mitochondrial transport along MTs by restricting radial displacement of MTs. Thus, mitochondrial movements in aged and neurodegenerative axons would be affected in a more complicated manner.

AT8 reactivity has been frequently used as an indicator of hyperphosphorylation of Tau in AD brains or other tauopathies (Stoothoff and Johnson, 2005; Hanger et al., 2009). Impairment of mitochondrial traffic is also a feature of tauopathies (Stokin et al., 2005; Lippens et al., 2007). An unanswered issue is whether abnormal Tau phosphorylation is caused by impaired organelle trafficking or if blocked transport is a consequence of abnormal phosphorylation. Using the phosphorylation mimic Tau 3D, we showed that Tau phosphorylation within the AT8 sites inhibited mitochondrial transport more effectively than in experiments carried out with Tau WT and Tau 3A. Because Tau 3A and 3D have similar phosphorylation profiles at other sites, the observed effect is likely caused by phosphorylation at Ser199/Ser202/Thr205. Thus, our results suggest that the increased phosphorylation of the AT8 sites in brains of Alzheimer's patients decreases mitochondrial transport in axons, leading to axonal degeneration. Our current study not only leads us to focus on the AT8 sites with regard to Alzheimer's therapeutics but also indicates the effectiveness of a similar strategy addressing other abnormal phosphorylation sites on mitochondrial movement.

References

Bereiter-Hahn J, Jendrach M (2010) Mitochondrial dynamics. Int Rev Cell Mol Biol 284:1–65.

Bershadsky AD, Gelfand VI, Svitkina TM, Tint IS (1978) Microtubules in mouse embryo fibroblasts extracted with Triton X-100. Cell Biol Int Rep 2:425–432.

Chen J, Kanai Y, Cowan NJ, Hirokawa N (1992) Projection domains of MAP2 and tau determine spacings between microtubules in dendrites and axons. Nature 360:674–677.

Darios F, Muriel MP, Khondiker ME, Brice A, Ruberg M (2005) Neurotoxic calcium transfer from endoplasmic reticulum to mitochondria is regulated by cyclin-dependent kinase 5-dependent phosphorylation of tau. J Neurosci 25:4159–4168.

Dixit R, Ross JL, Goldman YE, Holzbaur EL (2008) Differential regulation of dynein and kinesin motor proteins by tau. Science 319:1086–1089.

Dubey M, Chaudhury P, Kabiru H, Shea TB (2008) Tau inhibits anterograde axonal transport and perturbs stability in growing axonal neurites in part by displacing kinesin cargo: neurofilaments attenuate tau-mediated neurite instability. Cell Motil Cytoskeleton 65:89–99.

Ebneth A, Godemann R, Stamer K, Illenberger S, Trinczek B, Mandelkow E (1998) Overexpression of tau protein inhibits kinesin-dependent trafficking of vesicles, mitochondria and endoplasmic reticulum: implications for Alzheimer's disease. J Cell Biol 143:777–794.

Endo R, Saito T, Asada A, Kawahara H, Ohshima T, Hisanaga S (2009) Commitment of 1-methyl-4-phenylpyrinidinium ion-induced neuronal cell death by proteasome-mediated degradation of p35 cyclin-dependent kinase 5 activator. J Biol Chem 284:26029–26039.

Frappier TF, Georgieff IS, Brown K, Shelanski ML (1994) Tau Regulation of microtubule-microtubule spacing and bundling. J Neurochem 63:2288–2294.

Furuta K, Edamatsu M, Maeda Y, Toyoshima YY (2008) Diffusion and di-

rected movement: in vitro motile properties of fission yeast kinesin-14 Pkl1. J Biol Chem 283:36465–36473.
Goedert M, Jakes R, Vanmechelen E (1995) Monoclonal antibody AT8 recognises tau protein phosphorylated at both serine 202 and threonine 205. Neurosci Lett 189:167–169.
Hagiwara H, Yorifuji H, Sato-Yoshitake R, Hirokawa N (1994) Competition between motor molecules (kinesin and cytoplasmic dynein) and fibrous microtubule-associated proteins in binding to microtubules. J Biol Chem 269:3581–3589.
Hanger DP, Anderton BH, Noble W (2009) Tau phosphorylation: the therapeutic challenge for neurodegenerative disease. Trends Mol Med 15:112–119.
Hisanaga S, Hirokawa N (1989) The effects of dephosphorylation on the structure of the projections of neurofilament. J Neurosci 9:959–966.
Hollenbeck PJ, Saxton WM (2005) The axonal transport of mitochondria. J Cell Sci 118:5411–5419.
Hosokawa T, Saito T, Asada A, Fukunaga K, Hisanaga S (2010) Quantitative measurement of in vivo phosphorylation states of Cdk5 activator p35 by Phos-tag SDS-PAGE. Mol Cell Proteomics 9:1133–1143.
Ishiguro K, Takamatsu M, Tomizawa K, Omori A, Takahashi M, Arioka M, Uchida T, Imahori K (1992) Tau protein kinase I converts normal tau protein into A68-like component of paired helical filaments. J Biol Chem 267:10897–10901.
Jeganathan S, von Bergen M, Brutlach H, Steinhoff HJ, Mandelkow E (2006) Global hairpin folding of tau in solution. Biochemistry 45:2283–2293.
Jeganathan S, Hascher A, Chinnathambi S, Biernat J, Mandelkow EM, Mandelkow E (2008) Proline-directed pseudo-phosphorylation at AT8 and PHF1 epitopes induces a compaction of the paperclip folding of tau and generates a pathological (MC-1) conformation. J Biol Chem 283:32066–32076.
Jicha GA, Bowser R, Kazam IG, Davies P (1997) Alz-50 and MC-1, a new monoclonal antibody raised to paired helical filaments, recognize conformational epitopes on recombinant tau. J Neurosci Res 48:128–132.
Jicha GA, Berenfeld B, Davies P (1999) Sequence requirements for formation of conformational variants of tau similar to those found in Alzheimer's disease. J Neurosci Res 55:713–723.
Kaminosono S, Saito T, Oyama F, Ohshima T, Asada A, Nagai Y, Nukina N, Hisanaga S (2008) Suppression of mutant Huntingtin aggregate formation by Cdk5/p35 through the effect on microtubule stability. J Neurosci 28:8747–8755.
Kanai Y, Takemura R, Oshima T, Mori H, Ihara Y, Yanagisawa M, Masaki T, Hirokawa N (1989) Expression of multiple tau isoforms and microtubule bundle formation in fibroblasts transfected with a single tau cDNA. J Cell Biol 109:1173–1184.
Kanungo J, Zheng Y, Rudrabhatla P, Amin N, Mishra B, Pant H (2011) Deregulation of cytoskeletal protein phosphorylation and neurodegeneration. In: Advances in neurobiology: cytoskeleton of the nervous system (Nixon RA and Yuan A, eds), pp 297–324. New York: Springer.
Kimura T, Yamashita S, Fukuda T, Park JM, Murayama M, Mizoroki T, Yoshiike Y, Sahara N, Takashima A (2007) Hyperphosphorylated tau in parahippocampal cortex impairs place learning in aged mice expressing wild-type human tau. EMBO J 26:5143–5152.
Kinoshita E, Kinoshita-Kikuta E, Takiyama K, Koike T (2006) Phosphate-binding tag, a new tool to visualize phosphorylated proteins. Mol Cell Proteomics 5:749–757.
Knowles R, LeClerc N, Kosik KS (1994) Organization of actin and microtubules during process formation in tau-expressing Sf9 cells. Cell Motil Cytoskeleton 28:256–264.
Kumar S, Yin X, Trapp BD, Hoh JH, Paulaitis ME (2002) Relating interactions between neurofilaments to the structure of axonal neurofilament distributions through polymer brush models. Biophys J 82:2360–2372.
Lippens G, Sillen A, Landrieu I, Amniai L, Sibille N, Barbier P, Leroy A, Hanoulle X, Wieruszeski JM (2007) Tau aggregation in Alzheimer's disease: what role for phosphorylation? Prion 1:21–25.
Liu F, Li B, Tung EJ, Grundke-Iqbal I, Iqbal K, Gong CX (2007) Site-specific effects of tau phosphorylation on its microtubule assembly activity and self-aggregation. Eur J Neurosci 26:3429–3436.
Mandelkow EM, Thies E, Trinczek B, Biernat J, Mandelkow E (2004) MARK/PAR1 kinase is a regulator of microtubule-dependent transport in axons. J Cell Biol 167:99–110.
Marx A, Pless J, Mandelkow EM, Mandelkow E (2000) On the rigidity of the cytoskeleton: are MAPs cross-linkers or spacers of microtubules? Cell Mol Biol 46:949–965.
Marx A, Müller J, Mandelkow EM, Hoenger A, Mandelkow E (2006) Interaction of kinesin motors, microtubules, and MAPs. J Muscle Res Cell Motil 27:125–137.
Morel, M, Authelet M, Dedecker R, Brion JP (2010) Glycogen synthase kinase-3 and the P25 activator of cyclin dependent kinase 5 increase pausing of mitochondria in neurons. Neuroscience 167:1044–1056.
Morishima-Kawashima M, Hasegawa M, Takio K, Suzuki M, Yoshida H, Titani K, Ihara Y (1995) Proline-directed and non-proline-directed phosphorylation of PHF-tau. J Biol Chem 270:823–829.
Mukhopadhyay R, Hoh JH (2001) AFM force measurements on microtubule-associated proteins: the projection domain exerts a long-range repulsive force. FEBS Lett 505:374–378.
Planel E, Sun X, Takashima A (2002) Role of GSK-3β in Alzheimer's disease pathology. Drug Dev Res 56:491–510.
Plattner F, Angelo M, Giese KP (2006) The roles of cyclin-dependent kinase 5 and glycogen synthase kinase 3 in tau hyperphosphorylation. J Biol Chem 281:25457–25465.
Rankin CA, Sun Q, Gamblin TC (2005) Pseudo-phosphorylation of tau at Ser202 and Thr205 affects tau filament formation. Mol Brain Res 138:84–93.
Rochlin MW, Wickline KM, Bridgman PC (1996) Microtubule stability decreases axon elongation but not axoplasm production. J Neurosci 16:3236–3246.
Rudrabhatla P, Grant P, Jaffe H, Strong MJ, Pant HC (2010) Quantitative phosphoproteomic analysis of neuronal intermediate filament proteins (NF-M/H) in Alzheimer's disease by iTRAQ. FASEB J 24:4396–4407.
Saito T, Onuki R, Fujita Y, Kusakawa G, Ishiguro K, Bibb JA, Kishimoto T, Hisanaga S (2003) Developmental regulation of the proteolysis of the p35 cyclin-dependent kinase 5 activator by phosphorylation. J Neurosci 23:1189–1197.
Sakaue F, Saito T, Sato Y, Asada A, Ishiguro K, Hasegawa M, Hisanaga S (2005) Phosphorylation of FTDP-17 mutant tau by cyclin-dependent kinase 5 complexed with p35, p25, or p39. J Biol Chem 280:31522–31529.
Seeger MA, Rice SE (2010) Microtubule-associated protein-like binding of the kinesin-1 tail to microtubules. J Biol Chem 285:8155–8162.
Shahpasand K, Ahmadian S, Riazi GH (2008) A possible mechanism for controlling processive transport by microtubule-associated proteins. Neurosci Res 61:347–350.
Shemesh OA, Erez H, Ginzburg I, Spira ME (2008) Tau-induced traffic jams reflect organelles accumulation at points of microtubule polar mismatching. Traffic 9:458–471.
Stamer K, Vogel R, Thies E, Mandelkow E, Mandelkow EM (2002) Tau blocks traffic of organelles, neurofilaments, and APP-vesicles in neurons and enhances oxidative stress. J Cell Biol 156:1051–1063.
Stokin GB, Lillo C, Falzone TL, Brusch RG, Rockenstein E, Mount SL, Raman R, Davies P, Masliah E, Williams DS, Goldstein LS (2005) Axonopathy and transport deficits early in the pathogenesis of Alzheimer's disease. Science 307:1282–1288.
Stoothoff WH, Johnson GV (2005) Tau phosphorylation: physiological and pathological consequences. Biochim Biophys Acta 1739:280–297.
Stoothoff W, Jones PB, Spires-Jones TL, Joyner D, Chhabra E, Bercury K, Fan Z, Xie H, Bacskai B, Edd J, Irimia D, Hyman BT (2009) Differential effect of three-repeat and four-repeat tau on mitochondrial axonal transport. J Neurochem 111:417–427.
Su B, Wang X, Zheng L, Perry G, Smith MA, Zhu X (2010) Abnormal mitochondrial dynamics and neurodegenerative diseases. Biochim Biophys Acta 1802:135–142.
Sudo H, Baas PW (2010) Acetylation of microtubules influences their sensitivity to severing by katanin in neurons and fibroblasts. J Neurosci 30:7215–7226.
Takahashi S, Saito T, Hisanaga S, Pant HC, Kulkarni AB (2003) Tau phosphorylation by cyclin-dependent kinase 5/p39 during brain development reduces its affinity for microtubules. J Biol Chem 278:10506–10515.
Tatebayashi Y, Haque N, Tung YC, Iqbal K, Grundke-Iqbal I (2004) Role of tau phosphorylation by glycogen synthase kinase-3W in the regulation of organelle transport. J Cell Sci 117:1653–1663.
Thies E, Mandelkow EM (2007) Missorting of tau in neurons causes degeneration of synapses that can be rescued by MARK2/Par-1. J Neurosci 27:2896–2907.

Tokuoka H, Saito T, Yorifuji H, Wei F, Kishimoto T, Hisanaga S (2000) Brain-derived neurotrophic factor-induced phosphorylation of neurofilament-H subunit in primary cultures of embryo rat cortical neurons. J Cell Sci 113:1059–1068.

Trinczek B, Ebneth A, Mandelkow EM, Mandelkow E (1999) Tau regulates the attachment/detachment but not the speed of motors in microtubule-dependent transport of single vesicles and organelles. J Cell Sci 112:2355–2367.

Uchida A, Tashiro T, Komiya Y, Yorifuji H, Kishimoto T, Hisanaga S (2004) Morphological and biochemical changes of neurofilaments in aged rat sciatic nerve axons. J Neurochem 88:735–745.

Vershinin M, Carter BC, Razafsky DS, King SJ, Gross SP (2007) Multiple motor based transport and its regulation by Tau. Proc Natl Acad Sci U S A 104:87–92.

Vershinin M, Xu J, Razafsky DS, King SJ, Gross SP (2008) Tuning microtubule-based transport through flamentous MAPs: the problem of dynein. Traffic 9:882–892.

Verwer RW, Sluiter AA, Balesar RA, Baayen JC, Noske DP, Dirven CM, Wouda J, van Dam AM, Lucassen PJ, Swaab DF (2007) Mature astrocytes in the adult human neocortex express the early neuronal marker doublecortin. Brain 130:3321–3335.

Vossel KA, Zhang K, Brodbeck J, Daub AC, Sharma P, Finkbeiner S, Cui B, Mucke L (2010) Tau reduction prevents Abeta-induced defects in axonal transport. Science 330:198.

Wada Y, Ishiguro K, Itoh TJ, Uchida T, Hotani H, Saito T, Kishimoto T, Hisanaga S (1998) Microtubule-stimulated phosphorylation of tau at Ser202 and Thr205 by cdk5 decreases its microtubule nucleation activity. J Biochem 124:738–746.

Wang ZF, Li HL, Li XC, Zhang Q, Tian Q, Wang Q, Xu H, Wang JZ (2006) Effects of endogenous beta-amyloid overproduction on tau phosphorylation in cell culture. J Neurochem 98:1167–1175.

Watanabe A, Hasegawa M, Suzuki M, Takio K, Morishima-Kawashima M, Titani K, Arai T, Kosik KS, Ihara Y (1993) In vivo phosphorylation sites in fetal and adult rat tau. J Biol Chem 268:25712–25717.

Yu W, Baas PW (1994) Changes in microtubule number and lenghh during axon differentiation. J Neurosci 14:2818–2829.

Journal of the Neurological Sciences 301 (2011) 77–85

Contents lists available at ScienceDirect

Journal of the Neurological Sciences

journal homepage: www.elsevier.com/locate/jns

Clinicopathological study of diffuse neurofibrillary tangles with calcification With special reference to TDP-43 proteinopathy and alpha-synucleinopathy

Chikako Habuchi [a,b,*], Shuji Iritani [a,c], Hirotaka Sekiguchi [a], Youta Torii [a], Ryoko Ishihara [a], Tetsuaki Arai [c], Masato Hasegawa [d], Kuniaki Tsuchiya [e], Haruhiko Akiyama [c], Hiroto Shibayama [f], Norio Ozaki [a]

[a] Department of Psychiatry, Nagoya University Graduate School of Medicine, Tsurumai-cho, Showa-ku, Nagoya, Aichi-ken 466-8550, Japan
[b] Aichi Shiroyama Hospital, Nagoya, Japan
[c] Department of Psychogeriatrics, Tokyo Institute of Psychiatry, Tokyo Metropolitan Organization for Medical Research, Tokyo, Japan
[d] Department of Molecular Neurobiology, Tokyo Institute of Psychiatry, Tokyo Metropolitan Organization for Medical Research, Tokyo, Japan
[e] Department of Laboratory Medicine and Pathology, Tokyo Metropolitan Matsuzawa Hospital, Tokyo, Japan
[f] Asahigaoka Hospital, Aichi, Japan

ARTICLE INFO

Article history:
Received 15 April 2010
Received in revised form 24 October 2010
Accepted 25 October 2010
Available online 24 November 2010

Keywords:
Alzheimer's disease
Diffuse neurofibrillary tangles with calcification (DNTC)
Frontotemporal lobar degeneration
Non-Alzheimer degenerative dementia
Presenile dementia
Synucleinopathy
Tauopathy
TDP-43 proteinopathy

ABSTRACT

Diffuse neurofibrillary tangles with calcification (DNTC) is a relatively rare presenile dementia that clinically shows overlapping symptoms of Alzheimer's disease and frontotemporal lobar degeneration (FTLD). DNTC is pathologically characterized by localized temporal or frontotemporal atrophy with massive neurofibrillary tangles, neuropil threads and Fahr's-type calcification without senile plaques. We tried to clarify the molecular basis of DNTC by immunohistochemically examining the appearance and distribution of accumulated alpha-synuclein (aSyn) and TAR DNA-binding protein of 43 kDa (TDP-43) in the brains of 10 Japanese autopsy cases. We also investigated the clinically characteristic symptoms from the clinical charts and previous reports, and the correlations with neuropathological findings. The characteristic symptoms were evaluated using the Neuropsychiatric Inventory Questionnaire (NPI-Q). As a result, we confirmed the high frequency of neuronal cytoplasmic accumulation of aSyn (80%) and phosphorylated TDP-43 (90%) in DNTC cases. There was a significant correlation between some selected items of NPI-Q scores and the severity of the limbic TDP-43 pathology. The pathology of DNTC included TDP-43 and aSyn pathology with high frequency. These abnormal accumulations of TDP-43 might be involved in the pathological process of DNTC, having a close relationship to the FTLD-like psychiatric symptoms during the clinical course.

1. Introduction

Diffuse neurofibrillary tangles with calcification (DNTC) is a rare presenile dementia, thought to belong to tauopathy. Thus far, about 30 or more cases of DNTC have been reported, mainly from Japan. Clinically, patients with DNTC show overlapping symptoms with Alzheimer's disease (AD) and frontotemporal lobar degeneration (FTLD), including progressive memory disturbance, verbal disturbances, and personality changes (Fig. 1). Pathologically, DNTC is characterized by localized temporal or frontotemporal atrophy with massive neurofibrillary tangles (NFT), neuropil threads and Fahr's-type calcification without senile plaques [1,2].

Initially the diagnosis was neuropathologic. However, increasing knowledge about DNTC has made it possible for a clinical diagnosis also to be made [3,4]. At present, DNTC is considered a non-Alzheimer degenerative dementia, with frontotemporal lobar atrophy and frontal lobe syndrome which are characteristic in FTLD.

In 2006, two new discoveries were made in the research field of FTLD. One was the mutations of progranulin gene in familial FTLD with ubiquitin-positive, tau-negative neuronal cytoplasmic inclusions (FTLD-U) linked to chromosome 17 [5–7], and the other was TAR DNA-binding protein of 43 kDa (TDP-43) as a major component of ubiquitin-positive inclusions in most sporadic and familial cases of

Abbreviations: aSyn, alpha-synuclein; AD, Alzheimer's disease; AGD, argyrophilic grain disease; ALS, amyotrophic lateral sclerosis; DLB, Dementia with Lewy bodies; DN, dystrophic neurite; DNTC, diffuse neurofibrillary tangles with calcification; FTLD, frontotemporal lobar degeneration; FTLD-TDP, FTLD with ubiquitin-positive, tau-negative, TDP-43 positive neuronal cytoplasmic inclusions; FTLD-U, FTLD with ubiquitin-positive, tau-negative neuronal cytoplasmic inclusions; GB, Gallyas–Braak staining method; GCI, glial cytoplasmic inclusion; G-PDC, Guamanian ALS/parkinsonism–dementia complex; NFT, neurofibrillary tangles; NCI, neuronal cytoplasmic inclusion; NPI-Q, Neuropsychiatric Inventory Questionnaire; pTDP-43, phosphorylated TAR DNA-binding protein of 43 kDa; TDP-43, TAR DNA-binding protein of 43 kDa; Tx-PBS, PBS containing 0.3% Triton X-100.

* Corresponding author. Department of Psychiatry, Nagoya University Graduate School of Medicine, Tsurumai-cho, Showa-ku, Nagoya, Aichi-ken 466-8550, Japan. Tel.: +81 52 744 2282; fax: +81 52 744 2293.
E-mail address: habuchi@hm9.aitai.ne.jp (C. Habuchi).

0022-510X/$ – see front matter © 2010 Elsevier B.V. All rights reserved.
doi:10.1016/j.jns.2010.10.021

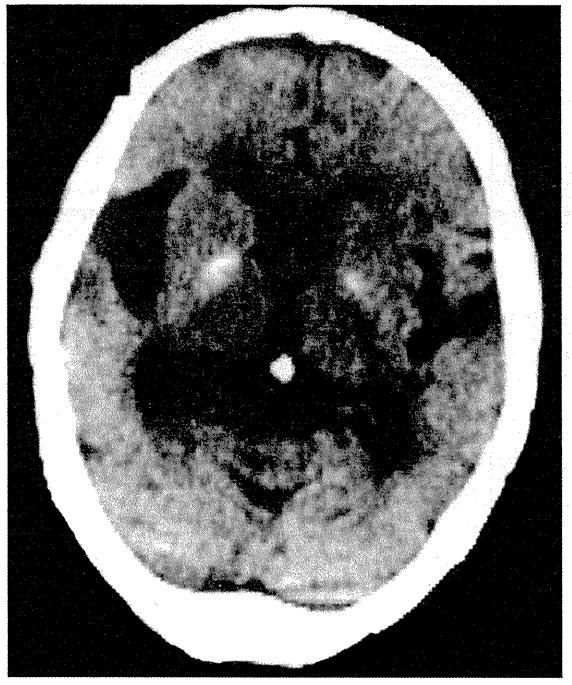

Fig. 1. Computed tomography of the brain showing bilateral atrophy of the frontal and temporal lobes with pallidal calcification (Case 8).

FTLD-U and amyotrophic lateral sclerosis (ALS) [8,9]. Subsequent studies have demonstrated the concurrence of TDP-43, tau, and alpha-synuclein (aSyn) pathology in other neurodegenerative disorders including AD, Dementia with Lewy bodies (DLB), Guamanian ALS/parkinsonism–dementia complex (G-PDC) and argyrophilic grain disease (AGD) [10–14]. However, it remains unclear whether or not these pathological proteins coexisted within the same neuron. In addition, although the clinical symptoms of DNTC have been attributed to a partial mixture of AD and FTLD [1], the way in which these neuropathological changes contribute to the clinical symptoms is not fully understood at present. Especially because the symptoms of DNTC clinically closely mimic those of FTLD, it is important to observe the pathology of DNTC specifically for a comparison with FTLD.

In order to clarify the proteinopathy of DNTC in this study, 1) we performed detailed immunohistochemical analyses of 10 Japanese DNTC cases, using phosphorylation-dependent anti-TDP-43 antibodies and anti aSyn antibodies. 2) Furthermore, we investigated the colocalization or non-colocalization of these proteins in DNTC using the technique of double-label immunofluorescence staining. 3) In addition, we considered the correlation between the clinical symptoms and the neuropathological findings based on the immunohistochemical investigations mentioned.

2. Materials and methods

2.1. Materials

Ten autopsied DNTC cases were examined (2 male, 8 female). The age at death ranged from 56 to 79 years (average 67.0 years). The weights of the brains ranged from 850 to 1265 g (average 1050 g) (Table 1). In all cases except one (Case 9), there were temporal or frontotemporal lobar atrophy, widespread NFTs, a paucity of plaques and pronounced Fahr's-type calcification in the basal nuclei or cerebellum, consistent with the neuropathological criteria of DNTC [2]. Case 9 was previously diagnosed as DNTC despite a lack of atrophy [15]. Detailed clinical data on some cases were previously reported elsewhere [1,16].

2.2. Methods

2.2.1. Tissue preparations

The brains were fixed with 10% buffered formalin and paraffin-embedded. Brain blocks of the frontal lobe, parietal lobe, temporal lobe, brainstem, and limbic region (including the amygdala, retro hippocampal formation, and parahippocampal gyrus), were cut into 5 μm-thick slices in the coronal section. All sections were stained with hematoxylin and eosin, Klüver–Barrera's method and Gallyas–Braak method (GB).

2.2.2. Immunohistochemistry

Immunohistochemistry was carried out using the avidin–biotin peroxidase complex technique (Vectastain ABC Kit; Vector Laboratories, Burlingame, CA, USA). Immunohistochemical staining was performed using anti-phosphorylated aSyn (Wako, concentration 1:3000), anti-TDP-43 (Protein Tech, 1:2000), and anti-phosphorylated TDP-43 (pTDP) (pS409/410 and pS403/404 [17], 1:1000, respectively). Some specimens were stained with anti-paired helical filament tau mouse monoclonal antibody (AT8; Innogenetics, Zwijndrecht, Belgium, 1:100). The sections were finally mounted in a glycerol-based medium and then observed using a light microscope. The Lewy body type, and the degree and distribution of Lewy pathology, were assessed by pathologic assessment and diagnostic criteria for DLB [18]. Furthermore, we assessed the TDP-43 pathology following the study of Amador-Ortiz, C. et al. [10]. Cases having more severe pathology outside of the temporal lobe were considered to have "diffuse" TDP-43 immunoreactivity. Cases with involvement relatively confined to the limbic lobe were referred to as "limbic." The TDP-43-positive structure was assessed using the following scheme: 0 = none, 1 = slight, 2 = mild, 3 = moderate, 4 = severe.

2.2.3. Double labeling immunofluorescence study

A double labeling immunofluorescence study was performed for pTDP-43 and phosphorylated tau, or for pTDP-43 and phosphorylated aSyn in Cases 2 and 8. The sections were incubated overnight at 4 °C in a cocktail of pS403/404 [17] and AT8 (Innogenetics, 1:100) or anti aSyn (Wako, 1:3000). After washing with PBS containing 0.3% Triton X-100 (Tx-PBS) for 30 min, the sections were incubated for 2 h at room temperature in a cocktail of fluorescein isothiocyanate-conjugated goat anti-mouse IgG (1:100; Millipore, Temecula, CA) and tetramethylrhodamine isothiocyanate-conjugated goat anti-rabbit IgG (1:100; Millipore). After washing, the sections were incubated in 0.1% Sudan Black B for 10 min at room temperature and washed with Tx-PBS for 30 min. The sections were coverslipped with Vectashield (Vector Laboratories) and observed with a confocal laser microscope (LSM5 PASCAL; Carl Zeiss MicroImaging GmbH, Jena, Germany).

2.2.4. Relationship between histopathology and clinical features

The clinically characteristic symptoms were investigated and summarized from the clinical charts and previous reports [1,15,16]. From this information, we assessed the neuropsychiatric symptoms of the 10 cases referring to the evaluation items of the Neuropsychiatric Inventory Questionnaire (NPI-Q) [19], in addition to cognitive and functional decline and verbal disturbance. We extracted three items from NPI-Q which are supposed to be marked, especially in FTLD cases: a) apathy or indifference, b) disinhibition (impulsiveness), and c) motor disturbance (pacing, compulsive behaviors). We investigated the statistical relationships between the scores of these characteristic items and the severity score of pathological findings. Statistical analyses were performed using Spearman's correlation coefficient method with $p<0.05$ considered statistically significant.

Table 1
Clinical features and neuropathological findings of 10 DNTC cases.

Case					1	2	3	4	5	6	7	8	9	10
Clinical diagnosis					PSD	AD	PSD	PiD	NANPD	AD+BD	NANPD	PiD	SPs	Sc
General information	Background	Sex			F	F	F	M	F	F	M	F	F	F
		Age at onset (years old)			46	49	51	52	56	56	59	64	65	NA
		Age at death (Duration years)			68(22)	57(8)	59(8)	56(4)	64(8)	79(17)	73(4)	72(8)	70(5)	72
		Cause of death			Pn	Inf	Inf	Pn	Pn	Inf	RnF	RnF	Pn	RnF
		Heredity			No	No	No	No	No	CVD, Sc	No	No	No	No
		Past history			No	No	Tb	No	No	Con	No	Men	No	SAH
	Brain	Weight (g)			850	1050	1140	1260	1000	920	1030	970	1265	1015
		Atrophy region			FL, TL	FL, TL	TL	FL, TL	TL	FL,TL	FL, TL	FL, TL	None	TL
Clinical findings	Memory disturbances (None, ±, +, ++)				++	+	+	±	+	+	+	+	±	None
	Verbal disturbances (None, +)				None	+	+	+	+	+	+	+	+	None
	Neurological symptoms				Pa, Ps	None	None	Pa	None	Dev	Pa, Ps	None	None	None
	†Personality changes	Three extracted items of NPI-Q score		Apathy	12	8	12	12	2	0	8	0	8	12
				Disinhibition	12	12	0	0	0	0	12	12	12	0
				Motor disturbance	0	0	12	8	0	0	12	8	0	8
				Total score	24	20	24	20	2	0	32	20	20	20
Pathological findings	††TDP-43 pathology	Distribution pattern			Limbic	Diffuse	Diffuse	Diffuse	Diffuse	Limbic	Diffuse	Diffuse	NA	Diffuse
		†††FTLD-TDP subtype			NA	2	2	2	2	NA	3	2	NA	2
		TDP-43 score	PC		0	1	0	0	0	0	3	0	0	1
			FC and TC	FC	NA	0	0	0	0	0	0	NA	0	0
				TC	0	2	1	3	2	0	4	2	0	4
				Total score	0	2	1	3	2	0	4	2	0	4
			LR	AMYG	4	NA	1	1	1	1	4	1	0	2
				HIP	1	2	1	0	0	1	1	2	0	1
				DG	0	1	0	0	0	0	0	0	0	0
				EC	0	3	1	3	1	0	2	2	0	2
				Total score	5	6	3	4	2	2	7	5	0	5
			FC, TC and LR total score		5	8	4	7	4	2	11	7	0	9
			BN		0	0	0	0	1	0	0	0	0	1
			Brain stem	SN	NA	NA	1	NA	1	NA	1	1	NA	1
	††††Lewy pathology	Distribution pattern			Limbic	NA	Limbic	Diffuse neocortical	Limbic	Diffuse neocortical	Diffuse neocortical	Diffuse neocortical	NA	Diffuse neocortical
		aSyn score	LR	HIP	2	0	3	4	3	4	4	4	0	4
				DG	0	0	0	1	0	3	1	0	0	0
			Brain stem	SN	NA	NA	2	NA	2	NA	3	2	NA	2
	Tau pathology	NFT (Braak Stage)			VI	VI	VI	VI	VI	VI	VI	VI	VI	VI

AD: Alzheimer's disease, AMYG: amygdala, aSyn: alpha-synuclein, BD: Binswanger's Disease, BN: basal nuclei, Con: convulsion, CVD: cerebrovascular disease, Dev: tongue deviation on protrusion, DG: hippocampal dentate gyrus, EC: entorhinal cortex, F: female, FC: frontal cortex, FL: frontal lobe, HIP: hippocampus, Inf: infection, LR: limbic region, M: male, Men: meningitis, NA: not available, NANPD: non-Alzheimer non-Pick dementia, NFT: neurofibrillary tangles, NPI-Q: Neuropsychiatric Inventory Questionnaire, Pa: parkinsonism, PC: parietal cortex, PiD: Pick disease, Pn: pneumonia, Ps: pyramidal sign, PSD: presenile dementia, RnF: renal failure, SAH: subdural hemorrhage, Sc: schizophrenia, SN: substantia nigra, SPs: senile psychosis, Tb: pulmonary tuberculosis, TC: temporal cortex, TDP-43: TDP-43: TAR DNA-binding protein of 43 kDa, TL: temporal lobe.

†Personality changes were assessed according to the Neuropsychiatric Inventory Questionnaire (score 0–12).

††The distribution pattern of TDP-43 was assessed following the study of Amador-Ortiz et al. [10]. The TDP-43-positive inclusions were assessed using the following scheme: 0: none, 1: slight, 2: mild, 3: moderate, and 4: severe.

†††FTLD-TDP subtype was assessed using the classification of Sampathu et al. [24].

††††The Lewy body type, and the degree (alpha-synuclein score (0–4)) and distribution of Lewy pathology, were assessed by pathologic assessment and diagnostic criteria for DLB (McKeith et al. [18]).

Statistical analyses were performed using Spearman's correlation coefficient method with $p<0.05$ considered statistically significant.

* $p>0.05$, ** $p<0.05$, *** $p>0.05$.

3. Results

3.1. Pathological findings

3.1.1. Tau pathology

In all cases, GB stain showed widespread and abundant NFTs throughout the neocortex and limbic system, especially the temporal cortex, hippocampus, and amygdala. The distribution pattern of NFTs indicated that all cases were classified as stages V or VI based on Braak and Braak staging [20].

3.1.2. The aSyn pathology

Alpha-Syn positive inclusions and neurites were observed in 8 cases (Cases 1, 3, 4, 5, 6, 7, 8, 10 in Table 1). The distribution of aSyn pathology was confined to the limbic region in 3 (Cases 1, 3, 5) of 8 cases, and extended to the neocortex in the other 5 cases. The former 3 cases were identified as the limbic type, and the latter 5 cases as the diffuse neocortical type, according to the classification of DLB by the study of McKeith et al. [18] (Table 1) (Fig. 2A). In the limbic region, aSyn-positive structures were present in dentate granule cells of the hippocampus in 3 cases (Cases 4, 6, 7) (Fig. 2B), in pyramidal neurons of CA2 and CA3 areas in 6 cases (Cases 3, 4, 6, 7, 8, 10) (Fig. 2C), and in the deep layer of the parahippocampal cortex in all 8 cases (Fig. 2D–F).

3.1.3. TDP-43 pathology

The pTDP-43 immunopositive structures were observed in 9 of 10 cases (Table 1). Regarding the distribution of pTDP-43 pathology, 2

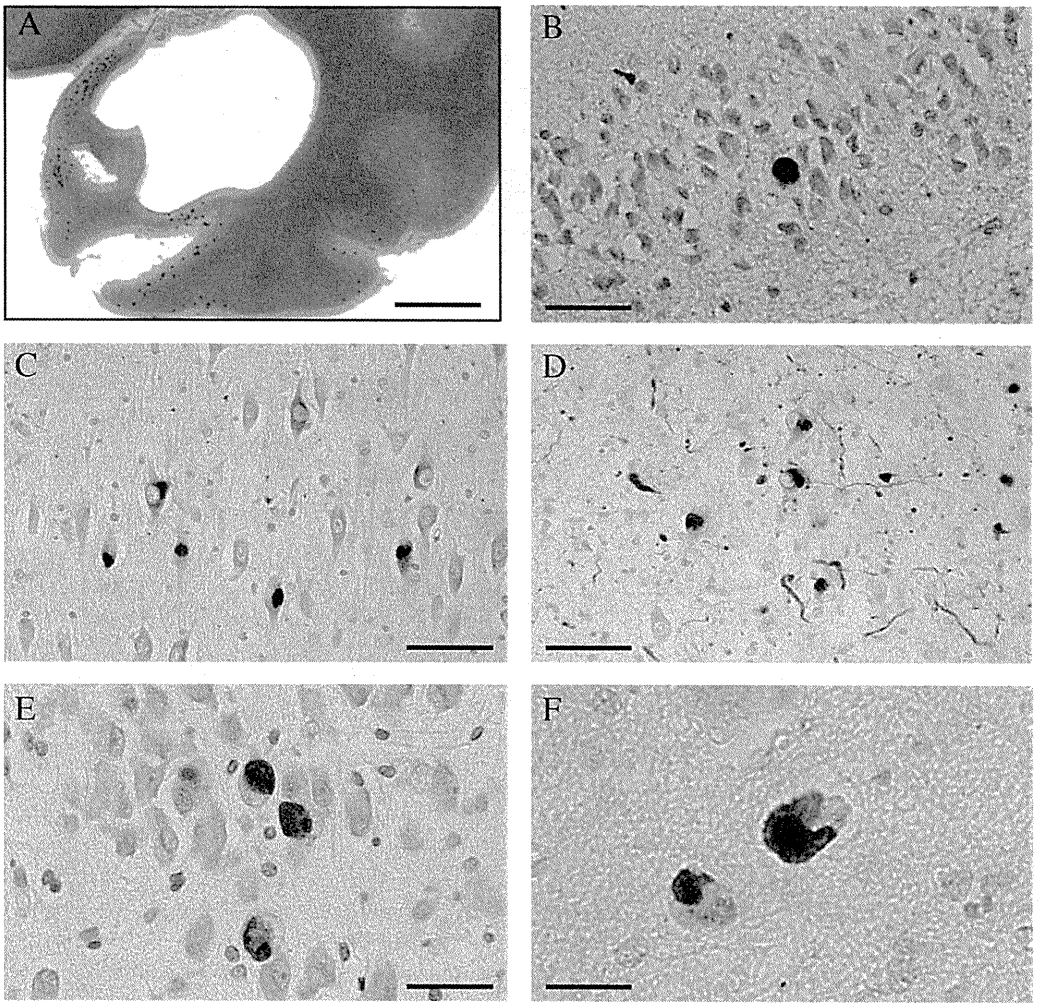

Fig. 2. A. Appearance of Lewy bodies and Lewy neurites in Case 8 (alpha-synuclein immunostaining: one dot indicates one Lewy body). B. Lewy bodies were observed in the dentate granule cell layer in the hippocampus (Case 6). C. Lewy bodies and neurites were observed in CA3 of Case 4. Scale bar = 50 μm. Lewy bodies were observed in the deep layer of the parahippocampal cortex (D (Case 7), E (Case 3), and F (Case 5)). Scale bar: A, 5 mm; B, C, 50 μm; D, E, and F, 20 μm.

of 9 cases showed pTDP-43 pathology confined to the limbic region, while the other 7 cases showed more widespread pTDP-43 pathology to the temporal neocortex. Of the 7 cases with pTDP-43 pathology in the neocortex, 6 cases (Cases 2, 3, 4, 5, 8, 10) showed predominant neuronal cytoplasmic inclusions (NCIs) with a few dystrophic neurites (DNs) (Fig. 3A–D), while Case 7 showed abundant NCIs and DNs (Fig. 3H–J). Glial cytoplasmic inclusions (GCIs) were also observed in all 9 cases (Fig. 3 E–G). NCIs in the dentate granular cells were found only in one (Case 2) of 9 cases. No neuronal intranuclear inclusions were seen in any of the cases.

Neuronal cytoplasmic granular structures positive for pTDP-43 but negative for a commercial anti-TDP-43 antibody were observed in 6 cases (Cases 2, 4, 5, 7, 8, 10) (Fig. 3K, L). Four (Cases 2, 7, 8, 10) of these showed both pTDP-43 positive cytoplasmic granules and NCIs/GCIs, while 2 cases (Cases 4, 5) showed only granules.

3.1.4. Colocalization of TDP-43 and aSyn or Tau

In double labeling immunofluorescence of the sections of the hippocampal region, a scarce colocalization of pTDP-43 and phosphorylated aSyn or a scarce colocalization of pTDP-43 and phosphorylated tau was observed in neuronal cytoplasm with very low frequency. However, we did see partial colocalization of aSyn and pTDP-43 in some neuronal cytoplasmic inclusions in the deep layer of the entorhinal cortex, and partial colocalization of tau and pTDP-43 in some neuronal cytoplasmic inclusions and the dentate gyrus of the hippocampus. Upon double-immunofluorescent labeling of cytoplasmic inclusions, pTDP-43 was scarcely superimposed with aSyn or tau (Fig. 4).

3.2. Clinical features

The clinical features of each patient are summarized in Table 1. Basically, the main symptoms comprised memory disturbances, verbal disturbances, or personality and behavioral changes in all cases. The degree of memory disturbance was moderate to severe in 7 cases (Cases 1, 2, 3, 5, 6, 7, 8). Verbal disturbances were found in 8 cases. Of these, 3 cases (Cases 5, 7, 8) showed verbal symptoms similar to primary progressive non-fluent aphasia, while one case (Case 2) showed semantic dementia-like symptoms. Regarding neurological symptoms, pyramidal signs including Babinski's sign were observed in 2 cases (Cases 1, 7), and parkinsonism in 3 cases (Cases 1, 4, 7).

Neuropsychiatric symptoms, including personality and behavioral changes, were assessed according to NPI-Q. Regarding personality changes, the symptoms of apathy or indifference were severe in 4 cases (Cases 1, 3, 4, 10). The symptoms of disinhibition characterized by morbid impulsion and 'going my way' behavior (i.e., lack of consideration for the feelings of others) were severe in 5 cases (Cases 1, 2,

7, 8, 9). The symptoms of motor disturbances, including pacing and compulsive behavior, were severe in 2 cases (Cases 3, 7).

3.3. Clinical features and pathology

We examined the relationship between the clinical features and aSyn pathology or TDP-43 pathology. Three cases (Cases 4, 6, 7) showed a higher aSyn score with aSyn-positive inclusions in dentate granular cells in the hippocampus and were identified as the diffuse neocortical type. Such cases tended to have neurological symptoms, including rigidity and akinesia (Cases 4, 7 in Table 1).

Two cases with spontaneous features of parkinsonism and progressive cognitive decline (Cases 4, 7, in Table 1) satisfied the clinical diagnostic criteria of possible DLB [18], and were thought to be categorized as the diffuse neocortical type. Among five cases (Cases 3, 5, 7, 8, 10) with brainstem synuclein pathology, only one case (Case 7) clinically showed parkinsonism.

From the viewpoint of clinical characteristics and TDP-43 pathology, cases with frequent pTDP-43-positive NCIs/GCIs in the hippocampus and amygdala tended to show higher scores of certain items in the NPI-Q (Cases 1, 7 in Table 1).

There were no significant correlations between the score of limbic TDP pathology and the score of each extracted item (apathy, disinhibition, and motor disturbances) of NPI-Q focused on three main clinical feature-associated frontotemporal symptoms (Spearman's correlation coefficient; 0.190, 0.459, and 0.394, respectively, all with p-value$>$0.05). However, there was a significant correlation between the score of limbic TDP pathology and the combined score of these three extracted items (Spearman's correlation coefficient 0.573, p-value$<$0.05). In contrast, there was no correlation between the sum of the scores of those three extracted items of NPI-Q and the severity score of frontotemporal TDP pathology (Spearman's correlation coefficient 0.200, p-value$>$0.05), nor the severity score of frontotemporal and limbic total TDP pathology (Spearman's correlation coefficient 0.441, p-value$>$0.05).

4. Discussion

In this study, we found high frequencies of cerebral accumulation of TDP-43 (90%) and of aSyn (80%) in DNTC. The accumulation of both abnormal proteins was observed in the limbic region most frequently. The immunoreactivity of TDP-43 was observed to further extend to the neocortex, in almost all cases presenting TDP-43 pathology. In addition, a significant correlation between the sum of the scores of certain question items of the NPI-Q and the score of the limbic TDP-43 pathology suggests that the abnormality of TDP-43 plays an important role in the pathological process and FTLD-like symptoms of DNTC.

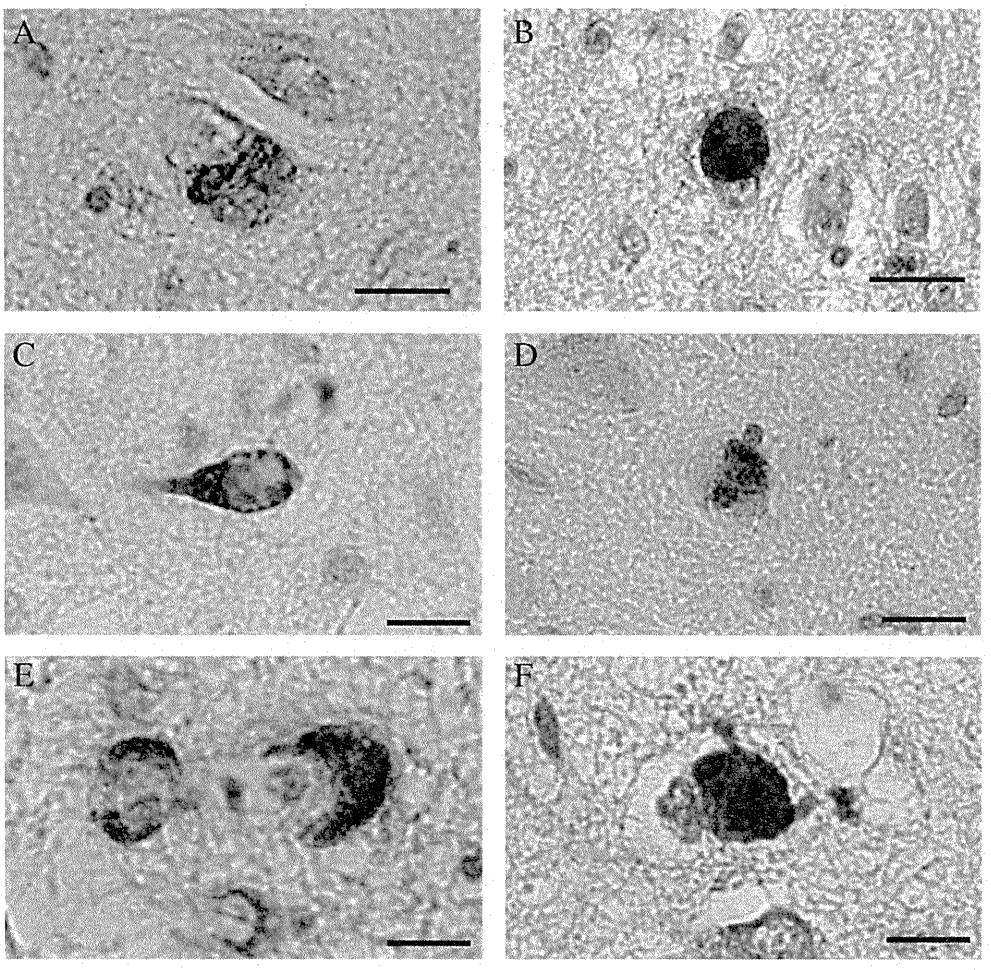

Fig. 3. NCIs were seen in the CA2 areas of Case 8 (A) and Case 1 (B) (anti-pTDP-43). NCIs were seen in the CA2 areas of Case 7 (C) and Case 8 (D) (anti-TDP-43). E. GCI-like structures were observed in the deep layer of the parahippocampal cortex in Case 7 (anti-pTDP). GCI was seen in the CA2 area (F) and CA3 area (G) of Case 2 (anti-pTDP). GCI-like structures and DNs were observed in the deep layer of the middle temporal gyrus (H), in the amygdala (I), and in the deep layer of the parahippocampal cortex (J) of Case 7 (anti-pTDP). Granular cytoplasmic pTDP-positive structures were observed in the CA2 area of Case 5 (K), and in the CA1 area of Case 4 (L) (anti-pTDP). Scale bar: A, C, E, and F, 10 μm; B, D, H, I, J, K, and L, 20 μm; G, 50 μm.

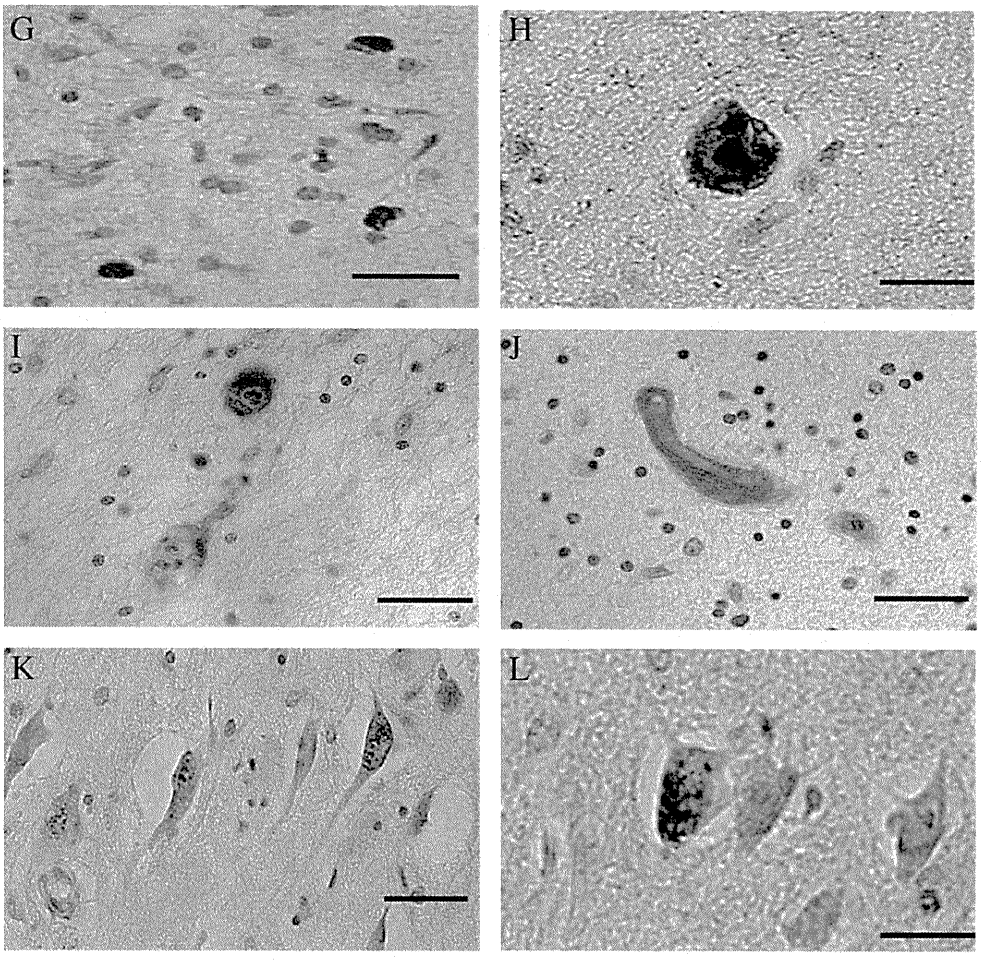

Fig. 3 (*continued*).

4.1. Alpha-Syn pathology in DNTC

The area of limbic region seemed to be the most vulnerable for aSyn pathology as well as tau pathology in DNTC (Table 1). These observations are consistent with the previous reports [21,22].

4.2. TDP-43 pathology in DNTC

We demonstrated a high frequency of TDP-43 pathology in 9 out of 10 DNTC cases (90%). Among the 9 cases having pTDP-43 pathology, 2 cases (Cases 1, 6) (22%) were identified as the 'limbic type,' while the other 7 cases (Cases 2, 3, 4, 5, 7, 8, 10) (77%) were "diffuse type," according to the classification by the study of Amador-Ortiz et al. [10]. The vulnerability of the limbic region to pTDP-43 accumulation found in our DNTC series was consistent with the previous reports of AD, DLB and AGD [10,11,13,14,23].

We mainly observed the pathology of DNTC for the purpose of comparison with FTLD. Recently, the TDP-43 pathology in FTLD has been classified into 4 subtypes according to the cortical TDP-43 pathology [24–26]. In the present study, 6 out of 7 cases (86%) with cortical TDP-43 pathology showed many NCIs/GCIs and sparse DNs, similar to the FTLD with ubiquitin-positive, tau-negative, TDP-43 positive neuronal cytoplasmic inclusions (FTLD-TDP), Type 2, using current terminology [27]. Only one case (Case 7) showed many NCI/GCIs and DNs, similarly to FTLD-TDP, Type 3. These findings of TDP-43 pathology in DNTC differ from those of AD and DLB cases, which almost all present Type 3 pathology [13,28,29].

In this point, the question arises as to whether this high frequency of TDP-43 pathology in DNTC cases represents a concurrent primary pathological process of FTLD-TDP or a secondary change occurring in susceptible neuronal populations. Although the high frequency of GCIs in DNTC is similar to the pathology of FTLD-TDP, Type 2, a simple coincidence of FTLD-TDP and DNTC seems unlikely based on our findings as follows. First, the main TDP-43 pathology in DNTC is similar to Type 2, but the frequency of TDP-43 positive NCIs in the dentate gyrus was low (one out of 9 cases; 11%) in our DNTC cases with TDP-43 immunoreactivity in comparison with those (about 80%) in FTLD-TDP, Type 2 [25,30]. Second, there are previous reports that 25–40% of FTLD-TDP cases with Type 2 pathology tend to be associated with clinical features of motor neuron disease [25,31]. In contrast, there was no case with Type 2-like pathology showing clinical features of motor neuron disease in our DNTC series.

Fig. 4. Double labeling immunofluorescence in Case 8 (A–F) demonstrates that most alpha-synuclein positive inclusions (green fluorescence in B, E) and pTDP-43 positive inclusions (red fluorescence in A, D) in the CA3 area of the hippocampus are independent (F), while there is partial colocalization of alpha-synuclein and pTDP-43 in some neuronal cytoplasmic inclusions in the deep layer of the entorhinal cortex (arrows in C). Double labeling immunofluorescence in Case 2 (G–L) demonstrates that most tau-positive neuropil threads (green fluorescence in H, K) and pTDP-43 positive inclusions (red fluorescence in G, J) in the entorhinal cortex are independent (L), while there is partial colocalization of tau and pTDP-43 in some neuronal cytoplasmic inclusions and the dentate gyrus of the hippocampus (arrows in I). Scale bar: A–L, 50 μm.

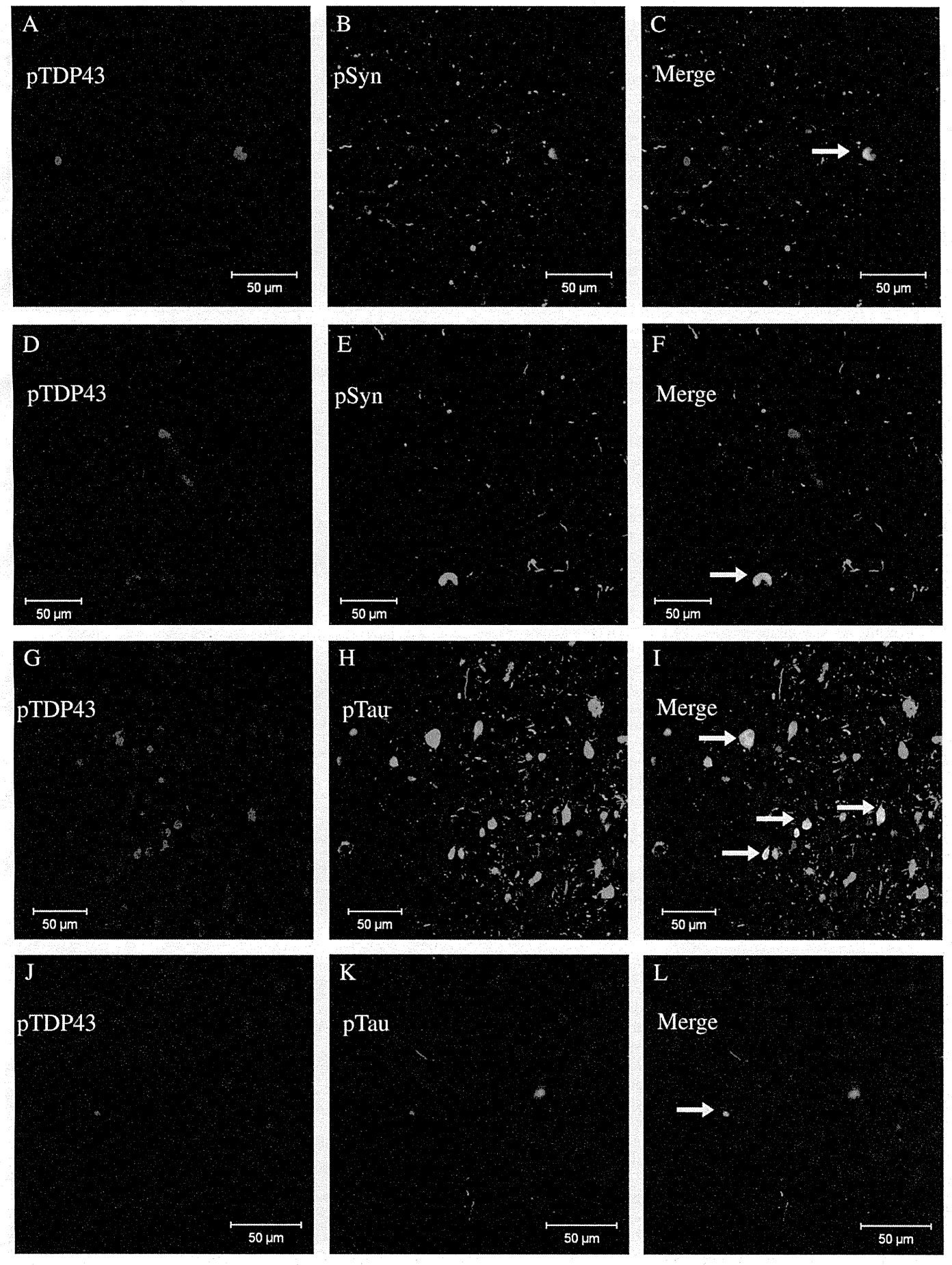
A
pTDP43
50 μm
B
pSyn
50 μm
C
Merge
50 μm
D
pTDP43
50 μm
E
pSyn
50 μm
F
Merge
50 μm
G
pTDP43
50 μm
H
pTau
50 μm
I
Merge
50 μm
J
pTDP43
50 μm
K
pTau
50 μm
L
Merge
50 μm

Therefore, it may be possible to speculate that TDP-43 pathology in DNTC has different characteristics from that of FTLD-TDP.

There arises another query concerning the possibility that the results in this study were driven by cross-reactive phospho-epitopes because the antibodies used for tau, aSyn and TDP-43 in this study were all phosphorylation-specific. Although there is some evidence of cross-reactivity with phosphorylated aSyn and phosphorylated tau [32], the anti-phosphorylated aSyn antibody used in this study did not immunostain NFT in AD brains, suggesting that it does not have cross-reactivity with phosphorylated tau.

Since the posttranslational modification is known to be a common motif in pathological protein accumulation in many neurodegenerative disorders and also this process can involve phosphorylation [33–36], the phosphorylation-dependent antibodies could mostly detect the pathological TDP-43 inclusions [13,17,37]. These mechanisms of phosphorylation might proceed in the pathologies of tau [34] or synuclein [38].

We found a scarce colocalization of pTDP-43 and tau and/or aSyn in some neuronal cytoplasmic inclusions in this study. Such a partial colocalization of tau (grain, or NFT), aSyn, and TDP-43 is consistent with that previously reported in AD, DLB, Pick's Disease, AGD, G-PDC and corticobasal degenerations to a varying degree [10–14,23]. As for the double-labeled cytoplasmic inclusions within the neuron, some reports [11,14] indicated that the TDP-43 was hardly superimposed with tau or observed only in a part of tau-positive cytoplasmic inclusions in AD or AGD based on double confocal microscopic observation. Also in this study, pTDP-43 scarcely coexisted with tau in neuronal cytoplasmic inclusions. These facts suggested that the pathway of appearance of the TDP-43 pathology might be different from that of the tau pathology but could relate closely in some way to tau proteinopathy of neurodegenerative diseases including DNTC.

It is possible that these findings were resulted from a non-specific vulnerability of the limbic region against these proteinopathies. However, there may be common factors or mechanisms that affect the conformation or modification of those proteins, leading to their intracellular accumulation. Especially, it was interesting to note that the results of the present study further supported the previous report that indicated similarity between DNTC and G-PDC [39]. Both disorders are assumed to be some type of endemic disease, and show frontotemporal atrophy and accumulation of tau, aSyn and TDP-43 without Amyloid β deposition. These findings could offer a hint toward understanding of the pathogenesis of these disorders.

4.3. Clinical features and pathology in DNTC

The phosphorylated aSyn pathology was observed in the brain stem of 5 cases of DNTC, but only one of these 5 cases had presented parkinsonism clinically. There seems to be a discrepancy between the presentation of parkinsonism and the pathological findings of phosphorylated aSyn appearance in DNTC.

There are some reports referring to an association between a specific clinical symptom and an underlying pathology in diverse degenerative disorders [40–43]. In our DNTC cases, the limbic region seemed to be the most vulnerable to abnormal accumulation of tau, aSyn and TDP-43. Thus, there is a possibility that not only accumulation of tau but also accumulation of aSyn and TDP-43 in the limbic region may be associated with early onset cognitive decline in DNTC. Indeed, in AD, concurrent TDP-43 pathology was reported to be associated with more severe cognitive decline [40].

In this study, we found a comprehensive association between pTDP-43 pathology and the frontotemporal symptoms (apathy, disinhibition, motor disturbances) in DNTC. Clinically, DNTC was diagnosed as FTLD because these three symptoms are representative and appear simultaneously to various degrees, so the integration of these three symptoms was very important for clinical assessment. Velakoulis, D. et al. recently reported that abnormalities in TDP-43 nuclear expression in the hippocampus were identified in patients with late-onset psychosis and a positive family history [44]. These findings suggest that abnormality of TDP-43 may be involved in the psychiatric symptoms of DNTC.

Meanwhile, there were some reports of DNTC without sufficient clinical or pathological assessment [4,45,46]. Cases of Fahr's syndrome with neuropsychological deficits and neuropsychiatric features have also been reported based on radiological findings [3,47,48]. More investigation will be needed to identify Fahr's syndrome as having the same background pathology of DNTC.

The association between basal ganglia calcification and psychotic symptoms has also been reported [49], but it remains unknown how the pathogenesis of calcification phenomenon concerns the psychosis. In the clinical setting, DNTC might pass unnoticed because it presents various clinical symptoms during the clinical course. Further studies on such cases from clinical, radiological and pathological standpoints might help elucidate the pathogenesis of DNTC.

5. Further assignment

We declare that there are some limitations of this study. Firstly, all the tissue samples were embedded in paraffin, so we could not perform molecular investigations including the Western Blotting test. Secondly, there were only a couple of sets of neuroimaging data of low resolution computed tomography available to this study, so we could not evaluate the association among the neuroimaging, neuropathology, and clinical symptoms. To address these issues, we are currently trying to upgrade the method for preserving tissue samples, and will acquire more neuroimaging data for a future prospective study.

References

[1] Shibayama H, Kobayashi H, Nakagawa M, Yamada K, Iwata H, Iwai K, et al. Non-Alzheimer non-Pick dementia with Fahr's syndrome. Clin Neuropathol 1992;11:237–50.
[2] Kosaka K. Diffuse neurofibrillary tangles with calcification: a new presenile dementia. J Neurol Neurosurg Psychiatry 1994;57:594–6.
[3] Modrego PJ, Mojonero J, Serrano M, Fayed N. Fahr's syndrome presenting with pure and progressive presenile dementia. Neurol Sci 2005;26:367–9.
[4] Nanda S, Bhatt SP, Pamula J, Woodruff WW, Fowler M, Miller D. Diffuse neurofibrillary tangles with calcification (DNTC): Kosaka–Shibayama disease in America. Am J Alzheimers Dis Other Demen 2007;22:535–7.
[5] Baker M, Mackenzie IR, Pickering-Brown SM, Gass J, Rademakers R, Lindholm C, et al. Mutations in progranulin cause tau-negative frontotemporal dementia linked to chromosome 17. Nature 2006;442:916–9.
[6] Cruts M, Gijselinck I, van der Zee J, Engelborghs S, Wils H, Pirici D, et al. Null mutations in progranulin cause ubiquitin-positive frontotemporal dementia linked to chromosome 17q21. Nature 2006;442:920–4.
[7] Gass J, Cannon A, Mackenzie IR, Boeve B, Baker M, Adamson J, et al. Mutations in progranulin are a major cause of ubiquitin-positive frontotemporal lobar degeneration. Hum Mol Genet 2006;15:2988–3001.
[8] Arai T, Hasegawa M, Akiyama H, Ikeda K, Nonaka T, Mori H, et al. TDP-43 is a component of ubiquitin-positive tau-negative inclusions in frontotemporal lobar degeneration and amyotrophic lateral sclerosis. Biochem Biophys Res Commun 2006;351:602–11.
[9] Neumann M, Sampathu DM, Kwong LK, Truax AC, Micsenyi MC, Chou TT, et al. Ubiquitinated TDP-43 in frontotemporal lobar degeneration and amyotrophic lateral sclerosis. Science 2006;314:130–3.
[10] Amador-Ortiz C, Lin WL, Ahmed Z, Personett D, Davies P, Duara R, et al. TDP-43 immunoreactivity in hippocampal sclerosis and Alzheimer's disease. Ann Neurol 2007;61:435–45.
[11] Higashi S, Iseki E, Yamamoto R, Minegishi M, Hino H, Fujisawa K, et al. Concurrence of TDP-43, tau and alpha-synuclein pathology in brains of Alzheimer's disease and dementia with Lewy bodies. Brain Res 2007;1184:284–94.
[12] Hasegawa M, Arai T, Akiyama H, Nonaka T, Mori H, Hashimoto T, et al. TDP-43 is deposited in the Guam parkinsonism–dementia complex brains. Brain 2007;130:1386–94.
[13] Arai T, Mackenzie IR, Hasegawa M, Nonoka T, Niizato K, Tsuchiya K, et al. Phosphorylated TDP-43 in Alzheimer's disease and dementia with Lewy bodies. Acta Neuropathol 2009;117:125–36.
[14] Fujishiro H, Uchikado H, Arai T, Hasegawa M, Akiyama H, Yokota O, et al. Accumulation of phosphorylated TDP-43 in brains of patients with argyrophilic grain disease. Acta Neuropathol 2009;117:151–8.
[15] Arai T, Kuroki N, Nizato K, Kase K, Iritani S, Ikeda K. An autopsy case of "diffuse neurofibrillary tangles with calcification", multiple infarctions and hyaline arteriosclerosis. No To Shinkei 1996;48:69–76.

[16] Shibayama H, Hoshino T, Kobayashi H, Iwase S, Takenouchi Y. An autopsy case of atypical senile dementia with atrophy of the temporal lobes—a clinical and histopathological report. Folia Psychiatr Neurol Jpn 1978;32:285–98.
[17] Hasegawa M, Arai T, Nonaka T, Kametani F, Yoshida M, Hashizume Y, et al. Phosphorylated TDP-43 in frontotemporal lobar degeneration and amyotrophic lateral sclerosis. Ann Neurol 2008;64:60–70.
[18] McKeith IG, Dickson DW, Lowe J, Emre M, O'Brien JT, Feldman H, et al. Diagnosis and management of dementia with Lewy bodies: third report of the DLB Consortium. Neurology 2005;65:1863–72.
[19] Kaufer DI, Cummings JL, Ketchel P, Smith V, MacMillan A, Shelley T, et al. Validation of the NPI-Q, a brief clinical form of the neuropsychiatric inventory. J Neuropsychiatry Clin Neurosci 2000;12:233–9.
[20] Braak H, Braak E. Neuropathological stageing of Alzheimer-related changes. Acta Neuropathol 1991;82:239–59.
[21] Yokota O, Terada S, Ishizu H, Tsuchiya K, Kitamura Y, Ikeda K, et al. NACP/alpha-synuclein immunoreactivity in diffuse neurofibrillary tangles with calcification (DNTC). Acta Neuropathol 2002;104:333–41.
[22] Hishikawa N, Hashizume Y, Ujihira N, Okada Y, Yoshida M, Sobue G. Alpha-synuclein-positive structures in association with diffuse neurofibrillary tangles with calcification. Neuropathol Appl Neurobiol 2003;29:280–7.
[23] Hu WT, Josephs KA, Knopman DS, Boeve BF, Dickson DW, Petersen RC, et al. Temporal lobar predominance of TDP-43 neuronal cytoplasmic inclusions in Alzheimer disease. Acta Neuropathol 2008;116:215–20.
[24] Sampathu DM, Neumann M, Kwong LK, Chou TT, Micsenyi M, Truax A, et al. Pathological heterogeneity of frontotemporal lobar degeneration with ubiquitin-positive inclusions delineated by ubiquitin immunohistochemistry and novel monoclonal antibodies. Am J Pathol 2006;169:1343–52.
[25] Mackenzie IR, Baborie A, Pickering-Brown S, Du Plessis D, Jaros E, Perry RH, et al. Heterogeneity of ubiquitin pathology in frontotemporal lobar degeneration: classification and relation to clinical phenotype. Acta Neuropathol 2006;112:539–49.
[26] Cairns NJ, Bigio EH, Mackenzie IR, Neumann M, Lee VM, Hatanpaa KJ, et al. Neuropathologic diagnostic and nosologic criteria for frontotemporal lobar degeneration: consensus of the Consortium for Frontotemporal Lobar Degeneration. Acta Neuropathol 2007;114:5–22.
[27] Mackenzie IR, Neumann M, Bigio EH, Cairns NJ, Alafuzoff I, Kril J, et al. Nomenclature for neuropathologic subtypes of frontotemporal lobar degeneration: consensus recommendations. Acta Neuropathol 2009;117:15–8.
[28] Nakashima-Yasuda H, Uryu K, Robinson J, Xie SX, Hurtig H, Duda JE, et al. Co-morbidity of TDP-43 proteinopathy in Lewy body related diseases. Acta Neuropathol 2007;114:221–9.
[29] Uryu K, Nakashima-Yasuda H, Forman MS, Kwong LK, Clark CM, Grossman M, et al. Concomitant TAR-DNA-binding protein 43 pathology is present in Alzheimer disease and corticobasal degeneration but not in other tauopathies. J Neuropathol Exp Neurol 2008;67:555–64.
[30] Davidson Y, Amin H, Kelley T, Shi J, Tian J, Kumaran R, et al. TDP-43 in ubiquitinated inclusions in the inferior olives in frontotemporal lobar degeneration and in other neurodegenerative diseases: a degenerative process distinct from normal ageing. Acta Neuropathol 2009;118:359–69.
[31] Josephs KA, Stroh A, Dugger B, Dickson DW. Evaluation of subcortical pathology and clinical correlations in FTLD-U subtypes. Acta Neuropathol 2009;118:349–58.
[32] Piao YS, Hayashi S, Hasegawa M, Wakabayashi K, Yamada M, Yoshimoto M, et al. Co-localization of alpha-synuclein and phosphorylated tau in neuronal and glial cytoplasmic inclusions in a patient with multiple system atrophy of long duration. Acta Neuropathol 2001;101:285–93.
[33] Ferrer I, Gomez-Isla T, Puig B, Freixes M, Ribe E, Dalfo E, et al. Current advances on different kinases involved in tau phosphorylation, and implications in Alzheimer's disease and tauopathies. Curr Alzheimer Res 2005;2:3–18.
[34] Luna-Munoz J, Chavez-Macias L, Garcia-Sierra F, Mena R. Earliest stages of tau conformational changes are related to the appearance of a sequence of specific phospho-dependent tau epitopes in Alzheimer's disease. J Alzheimers Dis 2007;12:365–75.
[35] Obi K, Akiyama H, Kondo H, Shimomura Y, Hasegawa M, Iwatsubo T, et al. Relationship of phosphorylated alpha-synuclein and tau accumulation to Abeta deposition in the cerebral cortex of dementia with Lewy bodies. Exp Neurol 2008;210:409–20.
[36] Cook C, Zhang YJ, Xu YF, Dickson DW, Petrucelli L. TDP-43 in neurodegenerative disorders. Expert Opin Biol Ther 2008;8:969–78.
[37] Schwab C, Arai T, Hasegawa M, Yu S, McGeer PL. Colocalization of transactivation-responsive DNA-binding protein 43 and huntingtin in inclusions of Huntington disease. J Neuropathol Exp Neurol 2008;67:1159–65.
[38] Saito Y, Kawashima A, Ruberu NN, Fujiwara H, Koyama S, Sawabe M, et al. Accumulation of phosphorylated alpha-synuclein in aging human brain. J Neuropathol Exp Neurol 2003;62:644–54.
[39] Tanabe Y, Ishizu H, Ishiguro K, Itoh N, Terada S, Haraguchi T, et al. Tau pathology in diffuse neurofibrillary tangles with calcification (DNTC): biochemical and immunohistochemical investigation. NeuroReport 2000;11:2473–7.
[40] Josephs KA, Whitwell JL, Knopman DS, Hu WT, Stroh DA, Baker M, et al. Abnormal TDP-43 immunoreactivity in AD modifies clinicopathologic and radiologic phenotype. Neurology 2008;70:1850–7.
[41] Yokota O, Tsuchiya K, Arai T, Yagishita S, Matsubara O, Mochizuki A, et al. Clinicopathological characterization of Pick's disease versus frontotemporal lobar degeneration with ubiquitin/TDP-43-positive inclusions. Acta Neuropathol 2009;117:429–44.
[42] Grossman M. Primary progressive aphasia: clinicopathological correlations. Nat Rev Neurol 2010; 6:88–97.
[43] Deramecourt V, Lebert F, Debachy B, Mackowiak-Cordoliani MA, Bombois S, Kerdraon O, et al. Prediction of pathology in primary progressive language and speech disorders. Neurology 2010; 74:42–49.
[44] Velakoulis D, Walterfang M, Mocellin R, Pantelis C, Dean B, McLean C. Abnormal hippocampal distribution of TDP-43 in patients with-late onset psychosis. Aust N Z J Psychiatry 2009;43:739–45.
[45] Nomoto N, Sugimoto H, Iguchi H, Kurihara T, Wakata N. A case of Fahr's disease presenting "diffuse neurofibrillary tangles with calcification". Rinsho Shinkeigaku 2002;42:745–9.
[46] Langlois NE, Grieve JH, Best PV. Changes of diffuse neurofibrillary tangles with calcification (DNTC) in a woman without evidence of dementia. J Neurol Neurosurg Psychiatry 1995;59:103.
[47] Hempel A, Henze M, Berghoff C, Garcia N, Ody R, Schroder J. PET findings and neuropsychological deficits in a case of Fahr's disease. Psychiatry Res 2001;108:133–40.
[48] Konupcikova K, Masopust J, Valis M, Horacek J. Dementia in a patient with Fahr's syndrome. Neuro Endocrinol Lett 2008;29:431–4.
[49] Ostling S, Andreasson LA, Skoog I. Basal ganglia calcification and psychotic symptoms in the very old. Int J Geriatr Psychiatry 2003;18:983–7.

NEUROPATHOLOGY

Neuropathology 2011; **31**, 135–143 doi:10.1111/j.1440-1789.2010.01152.x

Original Article

Gray matter lesions in Nasu-Hakola disease: A report on three autopsy cases

Naoya Aoki,[1,6] Kuniaki Tsuchiya,[1,2] Takashi Togo,[6] Zen Kobayashi,[1,3] Hirotake Uchikado,[6] Omi Katsuse,[6] Kyoko Suzuki,[6] Hiroshige Fujishiro,[4] Tetsuaki Arai,[1] Eizo Iseki,[4] Midori Anno,[5] Kenji Kosaka,[7] Haruhiko Akiyama[1] and Yoshio Hirayasu[6]

[1]Tokyo Institute of Psychiatry, [2]Department of Laboratory Medicine and Pathology, Tokyo Metropolitan Matsuzawa Hospital, [3]Department of Neurology and Neurological Science, Graduate School, Tokyo Medical and Dental University, [4]Department of Psychiatry, Juntendo Tokyo Koto Geriatric Medical Center, Juntendo University School of Medicine, [5]Department of Neurology, Tokyo Metropolitan Matsuzawa Hospital, Tokyo, [6]Department of Psychiatry, Yokohama City University School of Medicine and [7]Hoyu Hospital, Yokohama, Japan

Nasu-Hakola disease is an autosomal recessively inherited disease characterized by lipomembranous polycystic osteodysplasia and sclerosing leukoencephalopathy. While white matter lesions prominent in the brain have been reported in the literature, gray matter lesions have not received particular attention. In this study, we examined three autopsy cases of Nasu-Hakola disease in order to focus specifically on gray matter lesions. The ages at onset of the three cases were 20, 23 and 29 years, and the disease durations were 29, 19 and 8 years, respectively. In addition to characteristic degeneration in the cerebral white matter, such as demyelination with conspicuous fibrillary gliosis and axonal changes, all three cases showed overt pathology in the gray matter. Neuronal loss with gliosis in the thalamus (particularly in the dorsomedial nucleus and anterior nucleus), caudate nucleus, putamen and substantia nigra was prominent in all cases, and the severity corresponded to the disease duration. The cerebral cortices were relatively preserved in all cases. One case showed neuronal loss and gliosis in the gray matter of the hippocampus, possibly due to repeated episodes of epileptic convulsions. These gray matter pathologies are considered to be responsible for some of the clinical manifestations of the disease, including extrapyramidal symptoms.

Correspondence: Takashi Togo, MD, PhD, Department of Psychiatry, Yokohama City University School of Medicine, 3-9 Fukuura, Kanazawa-ku, Yokohama 236-0004, Japan. Email: togo.takashi@gmail.com

Received 28 January 2010; revised 8 June 2010 and accepted 6 July 2010; published online 29 September 2010.

Key words: gliosis, gray matter lesions, Nasu-Hakola disease, neuronal loss, polycystic lipomembranous osteodysplasia with sclerosing leukoencephalopathy (PlOSL).

INTRODUCTION

Nasu-Hakola disease, also known as polycystic lipomembranous osteodysplasia with sclerosing leukoencephalopathy (PlOSL), was first reported at about the same time in Japan and Finland.[1–3] Subsequently, approximately 160 cases have been reported, mainly in these two countries.[4] This disease is a rare autosomal recessively inherited disease and is caused by structural defects in one of two genes encoding different subunits of the same receptor signaling complex, TREM2 and DAP12.[5,6] Both TREM2 and DAP12 form a signaling receptor complex in cells of myeloid lineage.[7,8] Dysfunction of the microglia and osteoclasts has been proposed to explain CNS and bone pathogenesis, since these cell types originate from the same myeloid lineage.[5] Its clinical features are characterized by pain in the limb bones, followed by pathological fractures and progressive dementia with prefrontal syndrome, pyramidal signs, extrapyramidal signs and apracti-aphasic symptoms. These symptoms progress steadily and are later accompanied by other symptoms, especially convulsions, eventually leading to death in middle age. The characteristic histological features are convoluted membranocystic structures observed in the systemic adipose tissues, including fatty marrow in the affected bones. In the brain, cerebral lesions are characterized by diffuse and symmetrical demyelination with conspicuous fibrillary gliosis and axonal changes in the white matter. However, to date, gray matter lesions have not received particular attention,

possibly due to the prominence of the white matter lesions. The purpose of this study was to reveal the distribution and severity of neuronal loss in gray matter lesions in three cases of Nasu-Hakola disease.

MATERIALS AND METHODS

Clinical history of the cases

The clinical history of the disease was verified by an independent interview with the primary caregiver. The age at onset was defined as the age at which the subject first showed obvious signs suggestive of skeletal involvement or personality change, and was estimated on the basis of family members' reports and hospital records. The three cases underwent neurological, psychological and radiological examinations.

Neuropathological examination

Brain tissue samples were fixed post-mortem with 10% formalin and embedded in paraffin. Ten-μm-thick sections from the frontal, temporal, parietal, insular and cingulate cortex, hippocampus, amygdala, basal ganglia, midbrain, pons, medulla oblongata and cerebellum were prepared. These sections were stained with HE, KB, PAS, Holzer stain, Bodian stain, methenamine silver stain and Gallyas-Braak stain. Genetic analysis was not performed, since no frozen sections were available.

Semi-qualitative assessment of neuronal loss

The distribution and severity of neuronal loss associated with gliosis was graded on a "–" to "+++" scale using the HE-, KB- and Holzer-stained sections: –, neither neuronal loss nor gliosis observed; +, mild neuronal loss and gliosis observed; ++, moderate neuronal loss and gliosis observed, but tissue rarefaction absent; +++, severe neuronal loss and gliosis observed with tissue rarefaction.

RESULTS

The clinical and pathological characteristics of the three cases are summarized in Tables 1 and 2. The detailed clinical course and a part of the conventional pathological findings of Case 3 have previously been reported.[9]

Case reports

Case 1

A Japanese woman developed ankle pain in her left leg at the age of 20 and roentgenograms revealed a transparent shadow in her tibia. There was no family history of related disease. Bone biopsy revealed membranocystic changes

Table 2 Gray matter pathologies of the three cases

	Case 1	Case 2	Case 3
Brain weight (g)	840	910	1010
Neuronal loss			
Cerebral cortex	–	–	–
Hippocampus	+++	–	–
Amygdaloid nucleus	++	NA	–
Nucleus basalis of Meynert	NA	NA	–
Caudate nucleus	+++	+++	+
Putamen	++	++	+
Globus pallidus	–	NA	–
Thalamus			
Dorsomedial nucleus	+++	+++	++
Anterior nucleus	+++	+++	–
Ventrolateral nucleus	++	++	–
Pulvinar nucleus	++	NA	NA
Substantia nigra	++	++	+
Locus coeruleus	–	–	–
Pontine nucleus	–	–	–
Dentate nucleus of cerebellum	–	–	–
Hypoglossal nucleus	–	–	–
Dorsal nucleus of vagus	–	–	–
Inferior olivary nucleus	–	–	–

The degrees of neuronal loss were graded on "–" to "+++" scale using the HE, KB and Holzer-stained sections: –, neither neuronal loss nor gliosis observed; +, mild neuronal loss and gliosis observed; ++, moderate neuronal loss and gliosis observed, but tissue rarefaction absent; +++, severe neuronal loss and gliosis observed, with tissue rarefaction. NA, not available.

Table 1 Summary of clinical features

	Case 1	Case 2	Case 3
Sex	Female	Male	Female
Heredity	–	+	+
Age at onset (years)	20	23	29
Age at death (years)	49	42	37
Disease duration (years)	29	19	8
Initial signs	Ankle pain	Personality change (talkative)	Forgetfulness, fatigue
Skeletal symptoms	+	+	–
Dementia	+	+	+
Pyramidal signs	+	+	+
Extrapyramidal signs	Brachybasia, tremor	Not described	Brachybasia, rigidity, tremor
Convulsion	+	+	+

compatible with Nasu-Hakola disease. Disinhibition was observed from the age of 25, leading to personality changes such as euphoria, silly attitude, hyperactivity and shamelessness. Also, a neurological examination revealed brachybasia, tremor, dysarthria and dysmetria. Brain CT scan at that age showed mild diffuse brain atrophy, predominantly in the frontal lobes, and calcification in the bilateral basal ganglia. At the age of 34, she developed a progressive cognitive decline with impairment of episodic memory for recent events and stereotyped behavior. At the age of 40, she had difficulty with daily activities and was admitted to hospital. Thereafter, she suffered repeated convulsions. At the age of 42, she became bedridden. Her tendon reflexes in her extremities were all hyperactive, and ankle clonus appeared around that time. She developed hypokinesia and decreased response to external stimuli. These conditions persisted for several years, and she died of pneumonia and ileus at the age of 49.

Case 2

A Japanese man developed personality change at the age of 23. His parents were consanguineous, and his elder brother and younger sister had been diagnosed with Nasu-Hakola disease. He became talkative and often changed jobs. He repeatedly committed criminal acts and was taken into police custody for shoplifting at the age of 30. At the age of 31, he slipped and broke his left hip. Roentgenograms revealed multiple cystic lesions in many bones, and a bone biopsy revealed membranocystic changes compatible with Nasu-Hakola disease. After that, he was unable to walk, became susceptible to fractures and broke several other bones. He was admitted to the neurological ward of a hospital at the age of 32. On admission, he showed euphoria, shamelessness, memory disturbance and disorientation. He was not given a full neurological evaluation because of his multiple bone fractures. At the age of 38, he became dumb and suffered convulsions. One year later, tube feeding was started for severe dysphagia. Thereafter his condition deteriorated, and he entered an apallic state. He developed respiratory failure and finally died of pneumonia at the age of 42. His clinical diagnosis was Nasu-Hakola disease.

Case 3

A Japanese woman had been well until the age of 29, when she first complained of forgetfulness and fatigue. Her parents were consanguineous by the marriage of first cousins, and her younger sister had been diagnosed with typical Nasu-Hakola disease with skeletal and neuropsychiatric syndromes and membranocystic lesions in the bones. Personality change was observed from the age of 30, and she was twice arrested on the charge of theft. She developed brachybasia at the age of 32. She was admitted to the neurological ward of a hospital at the age of 35. On admission, she showed euphoria, apathy, memory disturbance and disorientation. Neurological examination revealed brachybasia, dysarthria, rigidity, tremor, hyperactive deep tendon reflex, bilateral Babinski's sign, ankle clonus and urinary incontinence. She soon developed convulsions. Her syndromes progressively worsened, with marked euphoria, disturbance of attention, aspontaneity, perseveration, amnestic syndrome, disorientation and dementia. She died of ileus at the age of 37. During her clinical course, no skeletal involvement or X-ray abnormality in the bones were revealed. She was pathologically diagnosed as having Nasu-Hakola disease based on findings such as membranocystic lesions in the adipose tissues and leukodystrophy in the brain.

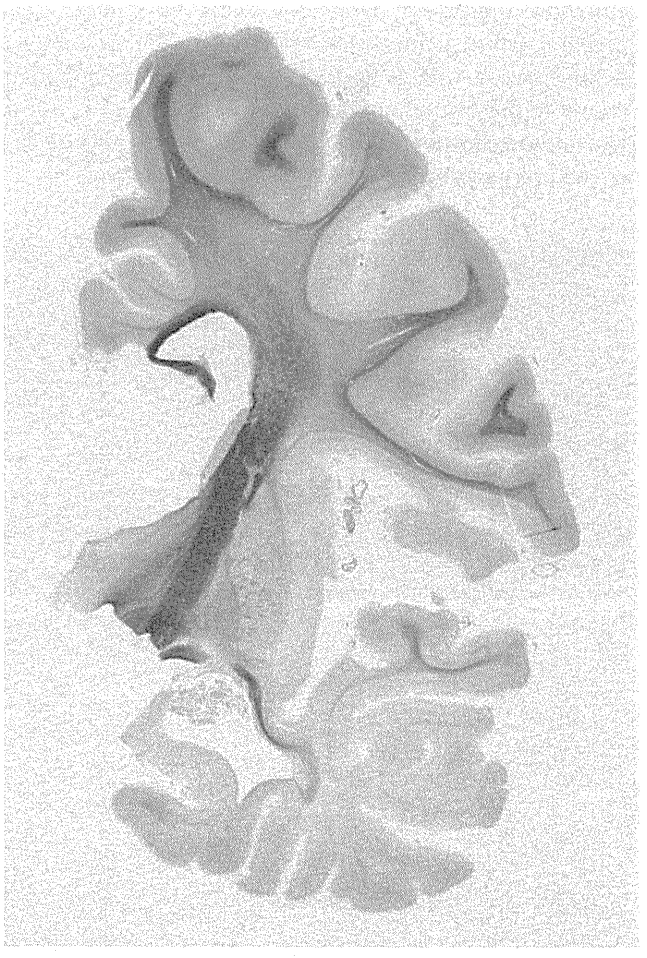

Fig. 1 Coronal section at the level of the globus pallidus. The caudate head is flattened and the thalamus is markedly atrophic. The lateral ventricles are extremely enlarged. Volume loss and myelin pallor were seen predominantly in the temporal lobe. KB stain. (Case 1)

Neuropathological findings

Macroscopic findings

All three cases showed very similar macroscopic findings. The brain weights (840, 910 and 1010 g) were subnormal, and generalized cerebral gyral atrophy with frontal accentuation was observed. In coronal sections, the cerebral cortex was generally of normal color and thickness, whereas the cerebral white matter appeared grayish and was decreased in volume. The changes in the white matter were more prominent in the frontal and temporal lobes. The lateral ventricle was dilated bilaterally. The basal ganglia, especially the caudate nucleus, were reduced in size (Fig. 1), and the thalamus was atrophic in Cases 1 and 2 but unremarkable in Case 3. The cerebellum and brain stems were unremarkable.

Histological findings of the white matter

All three cases showed a very similar distribution of demyelination consistent with Nasu-Hakola disease. The cerebral white matter showed diffuse and symmetrical demyelination with scattered axonal spheroids, predominantly in the frontal and temporal lobes. Fibrillary gliosis was noted in the demyelinating lesions. The pyramidal tract of the pons and medulla oblongata was also involved.

Histological findings of the gray matter

Neuronal loss and gliosis

All three cases showed neuronal loss and gliosis in the thalamus, caudate nucleus, putamen and substantia nigra (Figs 2–6). The characteristics of the gray matter lesions were the same in each case and region: neuronal loss and reactive gliosis were prominent in the affected gray matter and the severity of gliosis correlated with the severity of neuronal loss. The distribution and severity of neuronal loss is shown in Table 2. Among these areas, the thalamus was most severely affected in all cases.

In the thalamus, the most severe neuronal loss and gliosis were found in the dorsomedial nucleus, followed by the anterior nucleus. Neuronal loss in the dorsomedial nucleus was severe in Case 1 (Fig. 2B,F) and Case 2 (Fig. 2C,G), and was moderate in Case 3 (Fig. 2D,H). Neuronal loss in the anterior nucleus was severe in Cases 1 and 2, but was not observed in Case 3. Neuronal loss in the ventrolateral nucleus was moderate in Cases 1 and 2, but was not observed in Case 3. The pulvinar nucleus showed moderate neuronal loss in Case 1, but could not be examined in Cases 2 and 3. Neuronal loss in the caudate nucleus was severe in Case 1 (Fig. 3B,F) and Case 2 (Fig. 3C,G), but mild in Case 3 (Fig. 3D,H). Neu-

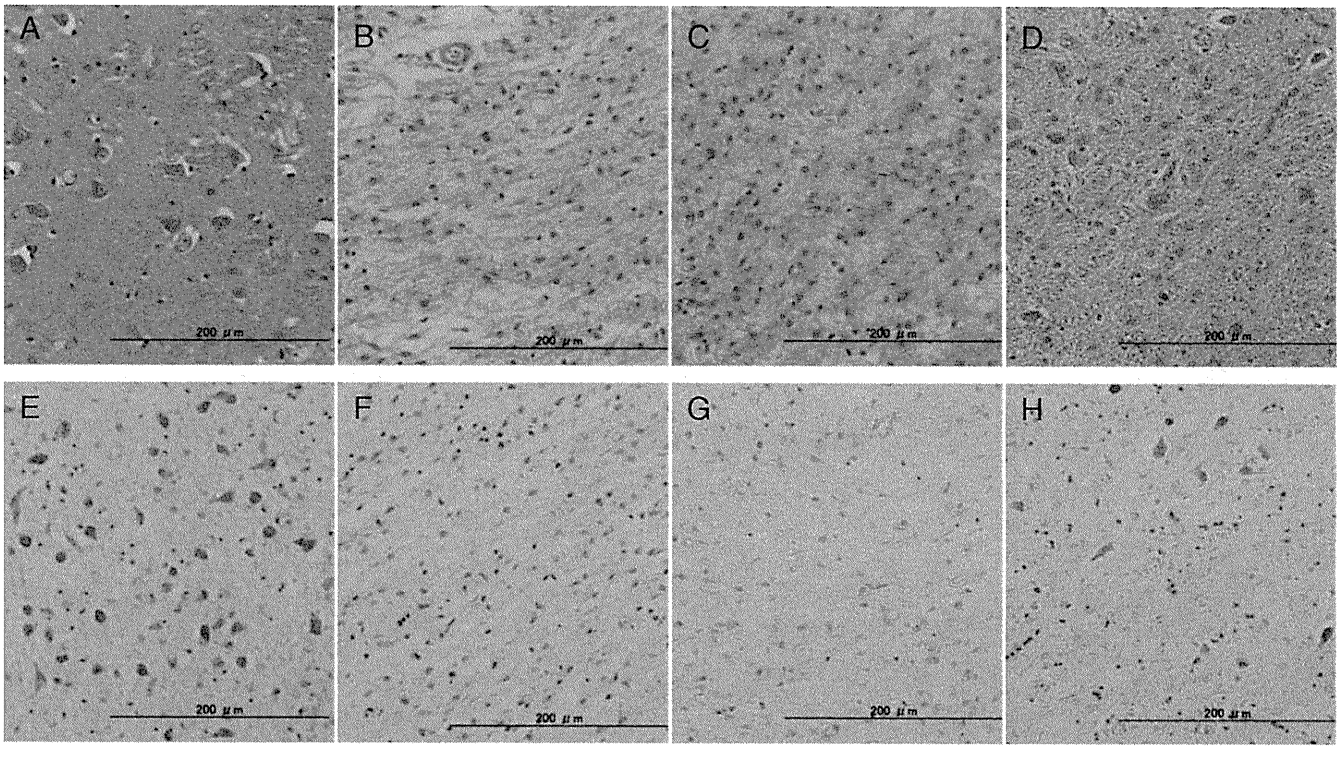

Fig. 2 Neuronal loss associated with glial proliferation in the thalamus (dorsomedial nucleus). Neither neuronal loss nor glial proliferation is noted in the normal control (A, E). Severe neuronal loss, remarkable glial proliferation, and tissue rarefaction are found in Case 1 (B, F) and Case 2 (C, G). Mild neuronal loss and glial proliferation are found, but no tissue rarefaction is seen in Case 3 (D, H). (A, D): HE stain; (E–H): KB stain. All scale bars = 200 μm.